university of groningen / faculty of science and engineering / mathematics and applied mathematics

The Hénon Map

Bachelor's Project Mathematics

July 2023

Student: T.J. Asbroek

First supervisor: dr. A.E. Sterk

Second assessor: dr. ir. R. Luppes

Abstract

The Hénon map is a two-dimensional quadratic map that, for some parameter values, has a strange attractor. This strange attractor has comparable properties to the Lorenz attractor and the strange attractors of many other systems. In this project, we discuss the map's history and its relation to the Lorenz system. We classify the stability of the fixed points of the Hénon map and identify curves in the parameter plane where period doubling bifurcations occur. Upon observing numerical evidence of a period doubling cascade, we identify the possibility for regions in the parameter plane where the map is chaotic. To further classify such regions, we rely on Lyapunov exponents. By means of a Lyapunov diagram, we then classify the system's stability and attractor type in a parameter plane, where we observe numerical evidence of a chaotic attractor. Lastly, we discuss the Hénon attractor and some of its properties. In particular, to further investigate its fractal properties, we give numerical estimates of its box-counting dimension and Lyapunov dimension. We conclude with a discussion regarding the relation that the Hénon attractor and the unstable manifold of one its saddle fixed points seem to have.

Contents

1 Introduction

In 1963, an article by Edward Lorenz titled *Deterministic Periodic Flow* was published (Lorenz, 1963). In this article, Lorenz is primarily concerned with deterministic hydrodynamical systems and their flow. Lorenz presents a mathematical proof that, under certain conditions, nonperiodic trajectories of such a system are necessarily unstable, meaning that trajectories starting very close to the nonperiodic trajectory, no matter how close, eventually separate from it by some distance. As a result, such systems where most trajectories are observed to be nonperiodic are quite unpredictable in the long run.

According to Lorenz, this result has far-reaching implications for many real world applications. For instance, based on the premise that atmospheric states are generally believed to evolve in a nonperiodic manner, this would imply that the slightest imperceptible change in the present state of the atmosphere is sufficient to cause its distant future to evolve into a completely different state. As a consequence, given the desire to predict future atmospheric states such as the weather, this implies that, even the slightest measurement error in its present state, which is arguably inevitable, is sufficient to make any prediction of a sufficiently distant future state effectively impossible (Lorenz, 1963).

To provide an illustrative example, Lorenz then gives a three-dimensional system that represents a simplified model of the convection and temperature variation of the flow of a two-dimensional fluid flow. For this system, which was later called the Lorenz system, Lorenz then presents numerical observations, for a particular set of parameter values, from which all trajectories are observed to be unstable and almost all appear to be nonperiodic. In addition, these trajectories appear to get trapped in some region of the phase space. In this region, the trajectories then seem to be attracted to a particular limit set that is observed to have some strange properties and a complex shape (Lorenz, 1963).

In order to get a better understanding of this "strange" attractor and its properties, in the article titled *A two-dimensional mapping with a strange attractor* published in 1976 (Hénon, 1976), Michel Hénon proposes a simple two-dimensional quadratic map which appears to have similar properties to the Lorenz system. In addition, upon iteration of the map some initial points appear to diverge towards infinity whereas others are observed to stay bounded. For some parameter values, for the cases where successive iterations stay bounded, the sequence of points are observed to tend towards a strange attractor that has similar properties to the Lorenz attractor. In this way, the map was presented as a useful tool, more tractable to analysis, to be used to get a better understanding of the Lorenz system and its attractor. This map was later named the Hénon map and is the main subject of this project.

Although the Hénon map is essentially just a simple theoretical model that has no direct bearing on the physical world, its properties, and, in particular, the structure of its attractor are characteristic of the properties of attractors seen in many physical systems (Broer & Takens, 2009). For instance, the strange attractors of dissipative hydrodynamical systems, where dissipative means that the flow of the system contracts volumes, are often observed to consist of manifolds folded closely on top of each other in a multisheeted structure bearing resemblance to a Cantor set (Grassberger & Procaccia, 1983), which is also observed in the attractor of the Hénon map. Besides, due to the period doubling behavior observed upon variation of the parameters, the Hénon map appears to have a similar route to chaos as is often seen before the onset of turbulence (Eckmann & Ruelle, 1985). So despite its simple form, the Hénon map can be considered as an important tool to get a better understanding of chaos and strange attractors.

In this project, we aim to cover and numerically investigate properties of the Hénon map. Specifi-

cally, we further investigate the relation that the Hénon map and its attractor have to the Lorenz system and its attractor. This discussion is followed by the investigation of its fixed points and the period doubling behaviour observed upon variation of parameter. Then, which can be considered as the main section of this project, using numerical methods, we classify the system's stability and attractor type in a parameter plane by means of Lyapunov exponents. Lastly, we conclude with a brief discussion on the fractal properties of the attractor along with its relation to the unstable manifold of one its saddle fixed points.

Whilst discussing these topics, we aim to introduce the concepts required such that the material presented is relatively self contained. To this end, we start of with a preliminary section on dynamical systems where basic results and definitions are presented. Whenever a new concept is discussed, such as Lyapunov exponents or fractal dimension, we give a brief introduction to that respective topic. This is done to ensure that the results are accessible to people with a mathematical background comparable to that of mathematics bachelor students.

2 Preliminaries

For the material and results discussed in this project some background theory is required. This section gives a brief introduction to important definitions and results from the field of dynamical systems.

2.1 Dynamical Systems

Definition 2.1 (Dynamical System)**.** *A deterministic dynamical system is a tuple (M, T, ϕ), where M is a non-empty set called the state space, the time set $T \subset \mathbb{R}$ is an additive semi-group, and $\phi : M \times T \to M$ is an evolution operator satisfying:*

1. *$\phi(x, 0) = x$ for any $x \in M$;*
2. *$\phi(\phi(x, t_1), t_2) = \phi(x, t_1 + t_2)$ for any $x \in M$ and $t_1, t_2 \in T$.*

These last two properties are also referred to as the group property of the evolution operator (Broer & Takens, 2009).

The notion of determinism in the definition means that future states are uniquely determined by present states only and that there is no ambiguity about future states given its present state. Despite requiring that all future states are uniquely determined given its present state, the definition does not require that all past states are uniquely determined by the present state. Namely, the time set T only has to be an additive semi-group and not necessarily a group. However, for a dynamical system (M, T, ϕ) where T is also a group, past states are uniquely determined by present states as well.

Given a dynamical system (M, T, ϕ) and a state $x \in M$, we can also define a mapping $T \to M$ given by $t \mapsto \phi(x, t) =: \phi^t(x)$, which is also referred to as the evolution operator for the initial state $x \in M$. Moreover, by the group property of the evolution operator, these maps satisfy $\phi^{t_1+t_2}(x) = \phi^{t_2} \circ \phi^{t_1}(x)$. The image of this map for the entire time set T is also referred to as the trajectory or orbit of x. In the cases where T is a group, the image of this map for $T_{\geq 0}$ is referred to as its forward orbit. Similarly, for a fixed $t \in T$, we can define the map $\phi^t : M \to M$ given by $x \mapsto \phi^t(x) = \phi(x, t)$ (Broer & Takens, 2009; Pugh, 2017).

Usually the time set T is $\mathbb{R}, \mathbb{R}_+, \mathbb{Z}$ or $\mathbb{Z}_+$. In the two former cases, namely T is $\mathbb{R}$ or $\mathbb{R}_+$, we speak of continuous dynamical systems. Such continuous dynamical systems are usually given as solutions to systems of ordinary differential equations. For instance, given an ordinary differential equations $f : \mathbb{R}^n \to \mathbb{R}^n$ that is C^1 and Lipschitz, we can define a dynamical system $(\mathbb{R}^n, \mathbb{R}, \phi)$ where $\phi(x, .)$ is the global solution of

$$\frac{\partial}{\partial t}\phi(x, t) = f(x), \quad \phi(x, 0) = x.$$

In the latter two cases, whenever the time set T is $\mathbb{Z}_+$ or $\mathbb{Z}$, we speak of discrete dynamical systems. These systems are usually associated with a map. Namely given a non-empty set M and a map $F : M \to M$, we can define a dynamical system $(M, \mathbb{Z}_+, \phi)$ where $\phi(x, n) := F^n(x)$. In particular, when F is a bijection, we can replace the semi-group $\mathbb{Z}_+$ by the group $\mathbb{Z}$ and define $\phi(x, -n) := F^{-n}(x) := (F^{-1})^n(x)$ for $-n < 0$ (Broer & Takens, 2009; Pugh, 2017).

In some cases, different dynamical system can exhibit comparable behaviour and the dynamics might only differ up to a homeomorphism.

Definition 2.2 (Topological Conjugacy)**.** *We say two dynamical systems (M, T, ϕ) and (M', T, ϕ') are topologically conjugate if there exists a homeomorphism $h : M \to M'$ such that $h \circ \phi(x, t) = \phi'(h(x), t)$ for all $x \in M$ and $t \in T$ (Devaney, 2003).*

Whenever two systems are topologically conjugate, it follows that the dynamics of the systems are topologically the same differing only by a homeomorphism.

2.2 Stability

An important area of the study of dynamical systems is the study of their steady states, limit sets, and their general limiting behaviour. Since the Hénon map is a discrete dynamical system, we will mostly focus on definitions and results relevant for discrete dynamical systems. To ease notation, we often express a discrete dynamical system as a map $F : M \to M$ such that $\phi(x, n) = F^n(x)$ for $x \in M$ and $n \in T$ with $T = \mathbb{Z}_{\geq 0}$ or $\mathbb{Z}$. Since in such cases the system is essentially just an iterated map, the fixed points and periodic points of the map are of interest for the system.

Definition 2.3. *Let $F : M \to M$ be some map with M non-empty. A point $x \in M$ is said to be a fixed point of F if $F(x) = x$. A point $x \in M$ is said to be periodic if $F^n(x) = x$ for some $n \geq 1$. The least positive n such that $F^n(x) = x$ is said to be the the period of x (Devaney, 2003).*

It is not difficult to see that for for a fixed point $x \in M$ of F that $F^k(x) = x$ for any $k \geq 0$ and that a periodic point $x \in M$ of period n is a fixed point of F^n. Moreover, the least positive property of the period n, of a periodic point $x \in M$, ensures that $F^k(x)$ are all distinct periodic points of period n for $k = 0, \ldots n - 1$.

Definition 2.4. *A fixed point $x \in \mathbb{R}^n$ of a C^1 map $F : \mathbb{R}^n \to \mathbb{R}^n$ is called hyperbolic if none of the eigenvalues of the linearization DF_x of F at x lie on the unit circle, i.e., $|\lambda| \neq 1$ for all eigenvalues λ of DF_x. Similarly, a periodic point $x \in \mathbb{R}^n$ with period k is called hyperbolic if it is a hyperbolic fixed point of F^k (Devaney, 2003).*

Then, for a hyperbolic fixed point $x \in \mathbb{R}^n$ of $F : \mathbb{R}^n \to \mathbb{R}^n$, the fact that F is C^1 implies that the systems is, locally, well-approximated by its linearization. Hence, the eigenvalue spectrum of its linearization is indicative of the local behaviour of the system.

Theorem 2.5. *If x is an hyperbolic fixed point of $F : \mathbb{R}^n \to \mathbb{R}^n$ such that $|\lambda| < 1$ for all $\lambda \in \sigma(DF_x)$, then there exists some open neighbourhood U of x such that $F^n(y) \to x$ as $n \to \infty$ for any $y \in U$, where convergence is understood in the Euclidean norm.*

Proof. Suppose $x \in \mathbb{R}^n$ is some fixed point of $F : \mathbb{R}^n \to \mathbb{R}^n$ such that $|\lambda| < 1$ for all $\lambda \in \sigma(DF_x)$. Then $||DF_x|| = \rho(DF_x) < 1$, where the former is the operator norm and the latter the spectral radius, i.e, the largest absolute value eigenvalue. Also, since F is C^1, the eigenvalues of DF_x depend smoothly on x and there exists some $B_\delta(x)$ such that $||DF_{x'}|| < \alpha < 1$ for all $x' \in B_\delta(x)$ for some real constant α.

Now let $x' \in B_\delta(x)$. Then, since x is a fixed point of F,

$$\begin{aligned}
||F(x') - x|| &= ||F(x') - F(x)|| \\
&= || \int_0^1 \frac{d}{dt} F(tx' + (1-t)x) dt|| \\
&\leq \int_0^1 || \frac{d}{dt} F(tx' + (1-t)x)(t)|| dt \\
&= \int_0^1 ||DF_{tx'+(1-t)x}(x' - x)|| dt \\
&\leq \int_0^1 ||DF_{tx'+(1-t)x}|| \cdot ||x' - x|| dt \\
&< \int_0^1 \alpha ||x' - x|| dt \\
&= \alpha ||x' - x||,
\end{aligned}$$

where we implicitly used the triangle inequality, the chain rule, and the fact that $B_\delta(x)$ is a convex set. This implies that $F(x') \in B_\delta(x)$, since $||F(x') - x|| < \alpha ||x' - x|| < \delta$. Following the same line of reasoning, we can show that if $F^n(x') \in B_\delta(x)$ that then $||F^{n+1}(x') - x|| < \alpha ||F^n(x') - x||$, from which it follows, by means of induction, that $||F^n(x') - x|| < \alpha^n ||x' - x||$ and hence $||F^n(x') - x|| \to 0$ as $n \to \infty$. □

The proof above is an adaptation of the proof presented in Devaney, 2003. For cases where F is a diffeomorphism, we can obtain a useful corollary to this theorem.

Corollary 2.6. *Suppose $x \in \mathbb{R}^n$ is some hyperbolic fixed point of $F : \mathbb{R}^n \to \mathbb{R}^n$ such that $|\lambda| > 1$ for all $\lambda \in \sigma(DF_x)$, then there exists some open neighbourhood U of x such that $F^n(y) \to x$ as $n \to -\infty$ for any $y \in U$.*

Proof. Suppose $x \in \mathbb{R}^n$ is some fixed point of $F : \mathbb{R}^n \to \mathbb{R}^n$ such that $|\lambda| > 1$ for all $\lambda \in \sigma(DF_x)$. Then x is also a hyperbolic fixed point of F^{-1} and $|\lambda| < 1$ for all $\lambda \in \sigma((DF^{-1})_x)$. The result then follows by a direct application of 2.5. □

As a consequence of these results, we adopt the following definition for hyperbolic fixed points based on a classification of the respective eigenvalue spectrum of the linearization.

Definition 2.7. *Suppose x is a hyperbolic fixed point of $F : \mathbb{R}^n \to \mathbb{R}^n$.*

1. *x is said to be an attracting fixed point if all eigenvalues of DF_x have an absolute value less than 1.*
2. *x is said to be a repelling fixed point if all eigenvalues of DF_x have an absolute value greater than 1.*
3. *x is said to be a saddle point otherwise, i.e., at least one eigenvalue of $DF(x)$ has an absolute value less than 1 and at least one eigenvalue is greater than 1 in absolute value.*

The definition is similar for a period-k hyperbolic point x with F replaced by F^k, i.e. considering x as a fixed point of F^k (Devaney, 2003).

This classification of hyperbolic periodic points is in fact the same for all points in the periodic cycle.

Proposition 2.8. *Suppose $x \in \mathbb{R}^n$ is some k-periodic hyperbolic point of $F : \mathbb{R}^n \to \mathbb{R}^n$, then the classification of x based on definition 2.7 is the same for all points its periodic cycle.*

Proof. Suppose $x \in \mathbb{R}^n$ is some k-periodic hyperbolic point of $F : \mathbb{R}^n \to \mathbb{R}^n$, it suffices to show that $\sigma((DF^k)_x) = \sigma((DF^k)_{F^m(x)})$ for any $1 \leq m < k$. Let m be such that $1 \leq m < k$, then by the chain rule

$$\begin{aligned}(DF^k)_{F^m(x)} &= DF_{F^{k-1+m}(x)} \circ \cdots \circ DF_{F^m(x)} \\ &= DF_{F^{m-1}(x)} \circ \cdots \circ DF_x \circ DF_{F^{k-1}(x)} \cdots \circ DF_{F^m(x)},\end{aligned}$$

and that

$$(DF^k)_x = DF_{F^{k-1}(x)} \circ \cdots \circ DF_x.$$

The results then follows by repeated application of the fact that AB and BA have the same eigenvalues for $n \times n$ matrices A, B. □

The result of theorem 2.5 and proposition 2.8 then also implies that it makes sense to talk about periodic cycles as being attracting or repelling in accordance with the classification given in definition 2.7.

These limit sets that are attracting under forward-iteration, which are also referred to as attractors, are not limited to periodic cycles or fixed points. To more formally define such attractors, it is of interest to see what limiting behaviour forward orbits of specific initial points have.

Definition 2.9. *Let $F : \mathbb{R}^n \to \mathbb{R}^n$ and $x_0 \in \mathbb{R}^n$. The ω-limit set $\omega(x_0)$ of the orbit $\{F^n(x_0)\}$ defined by x_0 is given by*

$$\omega(x_0) = \{y \in \mathbb{R}^n : F^{n_j}(x_0) \to x \text{ for some subsequence } \{n_j\}_{j \geq 1} \subset \mathbb{Z}_{\geq 0}\}.$$

The definition is taken from Broer and Takens, 2009, and allows for a formal definition of attractors.

Definition 2.10. *Adopting the notation of 2.9, we say that an ω-limit set $\omega(x)$ for $x \in \mathbb{R}^n$ is an attractor, whenever there exists arbitrarily small neighbourhoods of $\omega(x)$ such that*

$$F^n(U) \subset U$$

for all $n \geq 1$, and that for any $y \in U$, we have

$$\omega(y) \subset \omega(x).$$

This second condition is equivalently stated as

$$\bigcap_{n=0}^{\infty} F^n(U) = \omega(x),$$

for that particular neighbourhood U (Broer & Takens, 2009).

Notice that with this definition, repelling periodic cycles and periodic cycles of saddle type are precluded from being an attractor despite being the ω-limit of any point in the periodic cycle. However, attracting periodic cycles are classified as attractors with this definition, which is of course desirable given the general intuition and connotation one might have with these terms.

In addition, defining an attractor in such a way also implies that there is some larger set of initial points that tend towards the attractor upon iteration of the map. This set is also commonly referred to as the basin of attraction of that attractor.

Definition 2.11. *Whenever Λ is an attractor, we define its basin of attraction $B(\Lambda)$ as*

$$B(\Lambda) = \{y \in \mathbb{R}^n : \omega(y) \subset A\},$$

which is an open set (Broer & Takens, 2009).

When studying the stability of dynamical systems and their respective limit sets, it is common to do so for a family of dynamical systems that depend on a set of parameters. Then at values where there is a qualitative or topological change in the behaviour of the system, such as a change in stability of a limit set or a topological change of an attractor, a bifurcation is said to occur. The study of such bifurcations in the field of dynamical systems is also referred to as bifurcation theory (Broer & Takens, 2009).

Lastly, it should be noted the the results and definitions in this section can also be extended to more general cases of discrete dynamical systems, defined by C^1 maps, such as $F : U \to U$ where $U \subset \mathbb{R}^n$ is some domain. However, for the purposes of the study of the Hénon map, the above definitions and results suffice since this map is a diffeomorphism of the euclidean plane $\mathbb{R}^2$.

2.3 Chaos

The concept of deterministic chaos is an important topic and active field of research in the study of dynamical systems. The precise definition of whenever a system or attractor is said to be chaotic is also something that varies, where some definitions require more restrictive conditions than others. Depending on the context, the nature of the definition of chaos might also have a more topological flavour, posing conditions on the geometry of attractors and limit sets, or rely on ergodic properties, concerning statistical properties of systems when they are considered as satisfying some probability measure in the long run (Devaney, 2003). Altough these definitions might differ, it usually always involves sensitivity to initial conditions and the unpredictability of orbits (Peitgen et al., 2004).

To provide some intuition for the concept of of chaos, we will present a topological definition of chaos presented by Devaney, 2003, where one of the conditions for chaos is sensitive dependence on initial conditions.

Definition 2.12 (Devaney's definition of sensitive dependence on initial conditions)**.** *Let $F : J \to J$ with $J \subset \mathbb{R}^n$. Then F is said to have sensitive dependence on initial conditions if there exists a $\delta > 0$ such that, for any $x \in J$ and any neighbourhood N of x, there exists $y \in N$ such that*

$$||F^k(y) - F^k(x)|| > \delta,$$

for some $k \geq 1$ (Devaney, 2003).

Aside from sensitive dependence on initial conditions, Devaney also requires that chaotic systems possess some degree of indecomposability, i.e., that the system does not reduce to two subsystems that do not interact and that can be separated with disjoint open sets. The proposed condition that intends to guarantee this is that of topological transitivity.

Definition 2.13. *Let $F : J \to J$ with $J \subset \mathbb{R}^n$. Then F is said to be topologically transitive if for any pair of open sets $U, V \subset J$, we have*

$$F^k(U) \cap V = \emptyset$$

for some $k \geq 1$ (Devaney, 2003).

Lastly, Devaney's defintion of chaos requires that there is some degree of regularity in the system, albeit not always observed. For this latter condition, it is required that periodic points are dense.

Definition 2.14 (Devaney's definition of chaos)**.** *Let $F : J \to J$ with $J \subset \mathbb{R}^n$. Then F is said to be chaotic if*

1. *F has sensitive dependence on initial conditions.*
2. *F is topologically transitive.*
3. *periodic points are dense in J.*

With this definition, an attractor $\Lambda \subset J$ is then said to be chaotic if $F|_\Lambda$ is chaotic (Devaney, 2003).

However, since dynamical systems are often investigated by means of numerical techniques, this topological definition of chaos and chaotic attractors is rather difficult to work with in practice. For example, Devaney's definition of sensitive dependence on initial conditions is rather restrictive since it puts conditions on all initial points in a set. In addition, the other two conditions also pose problems since the geometric study of dynamical systems and attractors is quite difficult (Eckmann & Ruelle, 1985).

For this reason, for the purposes of studying the dynamics of the Hénon map, we will not be working with this definition of sensitive dependence on initial conditions and of chaos. Rather, in order to define these concepts in a useful way for numerical investigation, we will rely on Lyapunov exponents to define sensitive dependence on initial conditions and classify what it means for an attractor to be chaotic.

3 The Map

The map was originally proposed by Michel Hénon in his 1976 paper *A Two-dimensional Mapping with a Strange Attractor* (Hénon, 1976). The purpose of the map was for it to be a simple mapping that possesses similar properties to the Lorenz system and its Poincaré map. Below, a short overview of the Lorenz system is provided followed by the actual mapping later named the Hénon map along with some of its properties.

3.1 The Lorenz System

The Lorenz system is a system of ordinary differential equation modelling the convection and temperature variation of a two-dimensional fluid flow. The system was presented by Edward Lorenz in his 1963 article *Deterministic Nonperiodic Flow* (Lorenz, 1963), where the equations determining the dynamics of the system are given by

$$\begin{aligned} x' &= \sigma(y + x), \\ y' &= (\rho - z)x - y, \\ z' &= xy - \beta z, \end{aligned} \tag{1}$$

where σ, ρ, β are parameters. For the interested reader, a detailed derivation of the equations can be found in the appendix of Broer and Takens, 2009.

In this article, Lorenz is primarily interested in deterministic continuous ordinary differential equations modelling the flow of dissipative hydrodynamical systems that stay in some bounded phase space, where dissipative means that the flow contracts volumes. In particular, as suggested by the title, the flow of nonperiodic trajectories of said systems. Here a nonperiodic trajectory $P(t)$ is a trajectory that is not periodic, i.e, there exists no $\tau > 0$ such that $P(t + \tau) = P(t)$ for all t, and that also is not quasi-periodic. Here a quasi-periodic trajectory $P(t)$ is a trajectory such that for any $\epsilon > 0$ and any $\tau_0 > 0$ there exists some $\tau > \tau_0$ such that $||P(t + \tau) - P(t)|| < \epsilon$ for all $t > t_1$ for some t_1. Actually, since periodic trajectories are also quasi-periodic, it suffices for a trajectory to not be quasi-periodic in order for it to be nonperiodic (Lorenz, 1963).

Given that trajectories of such systems are bounded, it follows that any trajectories $P(t)$ has certain limit points P_0 that it gets arbitrarily close to infinitely many often. In addition, given that the system is assumed to be smooth, it follows that $P(t)$ gets arbitrarily close to any point of the trajectory through P_0 infinitely many times, which implies that the entire trajectory through P_0, when considered as a set, is contained in the set of limit points of the trajectory $P(t)$. Such a trajectory contained in the set of limit points of the trajectory $P(t)$ is said to a limiting trajectory of $P(t)$. Then, if $P(t)$ is contained in its own set of limiting trajectories, i.e., it revisits any point previously visited arbitrarily closely and infinitely many often, then the trajectory $P(t)$ is said to be central (Lorenz, 1963).

It is then shown, by means of a relatively straightforward deductive argument, that whenever a limiting-trajectory of a bounded trajectory $P(t)$ is stable that this necessarily implies that $P(t)$ is quasi-periodic. Here, a trajectory $P(t)$ with initial point $P(t_0)$ is stable if for any $\epsilon > 0$ there exists a $\delta > 0$ such that if another trajectory $P'(t)$ satisfies $||P'(t_0) - P(t_0)|| < \delta$ that then $||P'(t) - P(t)|| < \epsilon$ for all $t > t_0$, and a trajectory is unstable otherwise. From this it also follows that whenever a bounded trajectory $P(t)$ is nonperiodic that then no limiting-trajectories of $P(t)$ is stable. Hence, whenever $P(t)$ is a central nonperiodic trajectory, this also implies that $P(t)$ is necessarily unstable. A similar but weaker result is obtained for noncentral nonperiodic trajectories where it is mentioned that theoretically such trajectories can still be stable but that they likely do not have any bearing on reality (Lorenz, 1963).

According to Lorenz, this observation has far-reaching consequences for many real world applications. For instance, given the fact that atmospheric states are generally accepted to evolve in a nonperiodic manner, this implies that initial states differing only by negligible and imperceptible amounts can evolve, given a sufficiently large time-line, into completely different states. This would mean that even the slightest measurement error of the initial state, which is inevitable, is sufficient to make any prediction of a sufficiently distant future impossible (Lorenz, 1963).

Lorenz then proceeds to present the system given by 1 as an example of a simple model of a hydrodynamical system where, for certain parameter values, by means of numerical simulation, all solutions are found the unstable and almost all are found to be nonperiodic. In particular, for the parameter values $\sigma = 10, \rho = 28, \beta = 8/3$ some numerically approximated solutions are plotted where it is observed that these seem to tend towards an attractor with a complex shape and strange properties. Figure 1 shows a numerical approximation to a trajectory for these parameter values where this attractor can be observed.

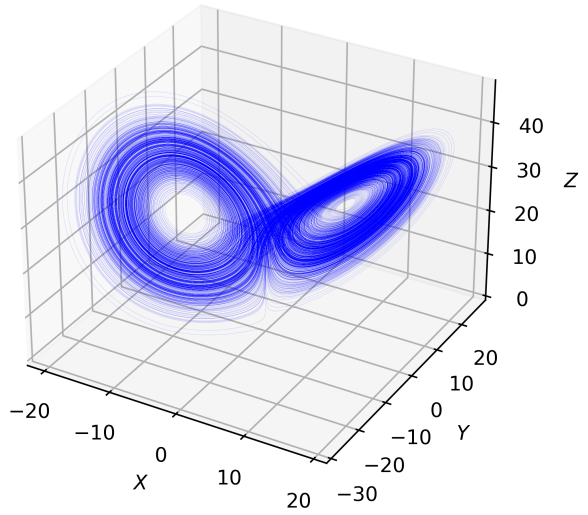

Figure 1: Lorenz attractor for $\sigma = 10, \rho = 28, \beta = 8/3$. One million iterations with $\Delta t = 0.001$ using a second-order approximation procedure identical to the procedure used by Lorenz, 1963.

As noted by Hénon, 1976, the Lorenz system seems to have a bounded region R where the trajectories of the system eventually get trapped into. Then, due to the fact that the system is dissipative, this causes the flow of the system to contract R to the attractor which necessarily has measure zero as a result. Then, for the parameter values where the attractor assumes its complex shape, it was found by numerical experiments of Yves Pomeau in 1976, which were not published, that the system appears to stretch in one direction and fold over itself in the course of rotations around the attractor. The attractor then appears to consist of surfaces folded closely on top of each other in a manner bearing familiarity to a Cantor set (Hénon, 1976).

Then, in 1976, in the article titled *A Two-dimensional Mapping with a Strange Attractor*, Michel Hénon proposed a two-dimensional quadratic map that appears to have properties similar to that

of the Lorenz system (Hénon, 1976). In addition, for some parameter values the map appears to have a "strange" attractor that has similar properties to the Lorenz attractor. In this way, the map aims to provide a model, more tractable for purposes of mathematical analysis, to be used to get a better understanding of the Lorenz system and its attractor. In the next section, we briefly explain Hénon's reasoning used in the construction of the map along with the map itself and some of its properties that relate it to the Lorenz system and its attractor.

3.2 The Hénon Map

In order to derive a simplified model of the Lorenz system and its attractor, Hénon considered three steps. The first step was the consideration of the Poincaré map of the Lorenz attractor, which roughly speaking is a map that maps successive intersections of a trajectory with a hyperplane to each other. This reduces the dynamics of the three-dimensional continuous system to that of a two-dimensional discrete system. However, this would unfortunately still require the numerical integration of the original trajectories and the process of finding successive intersections with the hyperplane. To overcome this difficulty, the second step was the consideration that defining an explicit map would simplify the computation significantly. In addition, provided this map is chosen carefully, it can hopefully be constructed in a way such that it emulates some of the desired properties also seen in the Lorenz system. The last step then consist of an explicit construction of this map (Hénon, 1976).

The map is constructed as the composition of three maps, where each map aims to emulate a property observed in the Lorenz system. Motivated by the folding effect observed in the Lorenz system, the first map is

$$H'(x, y) = (x, y + 1 - ax^2),$$

where a is some folding parameter. The second map is then a contraction along the x-axis

$$H''(x, y) = (bx, y)$$

with $-1 < b < 1$ a contraction parameter, and, lastly, a reflection given by

$$H'''(x, y) = (y, x).$$

The composition $H_{a,b}(x, y) = H''' \circ H'' \circ H'(x, y)$ is then given by

$$H_{a,b}(x, y) = (y + 1 - ax^2, bx), \tag{2}$$

which was later named the Hénon map.

Figure 2 illustrates the effect of the folding of H', the contraction of H'', and the reflection H''' with $a = 1$ and $b = 0.5$. Figure 3 shows the folding and contraction effect of the map for different iterations with $a = 1.4$ and $b = 0.3$, which are the classic parameter values originally selected by Hénon. From figure 3, we observe that after a few iterations, the map seems to stretch a cube in one direction and contract it in the other direction. This then causes the cube to be deformed into a curve which appears to be folded on top of itself.

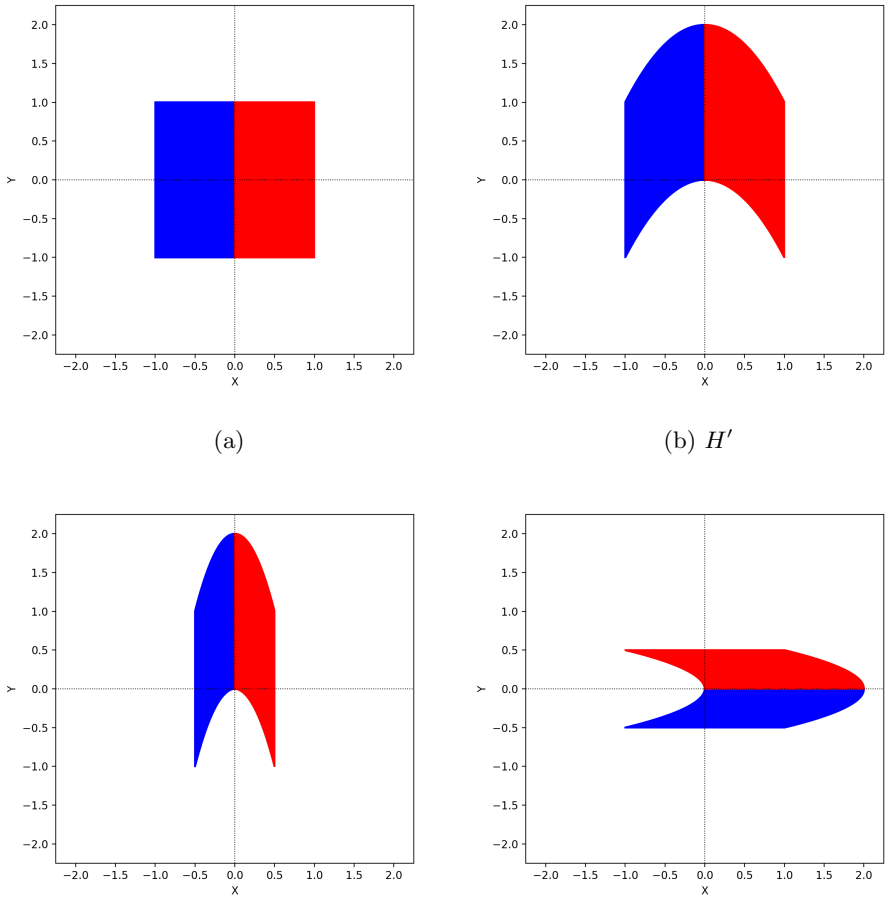

(a) (b) H'

(c) H'' (d) H'''

Figure 2: The maps H', H'', H''' applied sequentially to the unit square with $a = 1$, $b = 0.5$.

The linearization of the map is given by

$$DH_{a,b}(x, y) = \begin{pmatrix} -2ax & 1 \\ b & 0 \end{pmatrix}, \tag{3}$$

which has constant determinant $-b$. The result is that the map contracts areas by a constant factor $|b| < 1$ and reverses the orientation whenever $b > 0$. This property of contracting areas is desirable from the perspective of emulating the Lorenz system since this system is also dissipative (Hénon, 1976).

In addition, the map is a diffeomorphism from $\mathbb{R}^2$ to itself with inverse

$$H^{-1}_{a,b}(x, y) = \left(\frac{y}{b}, x - 1 + \frac{ay^2}{b^2} \right), \tag{4}$$

provided that b is nonzero. Since trajectories through a particular point of the Lorenz system are also unique, the existence of such an inverse is also a welcome property.

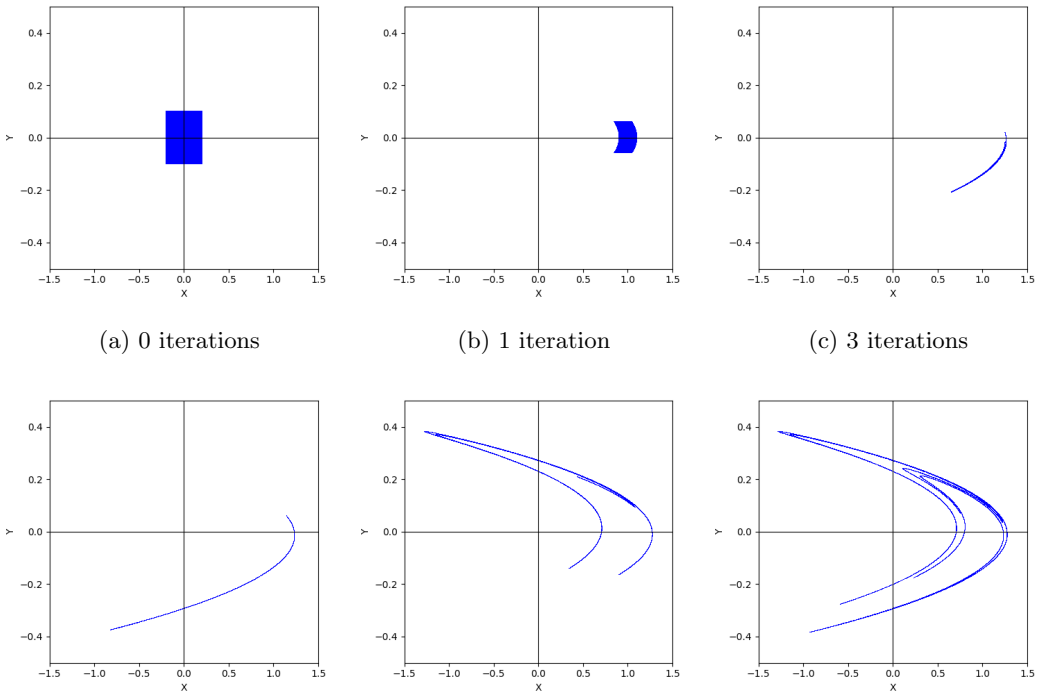

(a) 0 iterations (b) 1 iteration (c) 3 iterations

(d) 5 iterations (e) 10 iterations (f) 20 iterations

Figure 3: The effect of iterating the Hénon map with $a = 1.4$ and $b = 0.3$ for a set of initial points in a square.

The map has two fixed points given by

$$x_+ = \frac{-(1-b) + \sqrt{(1-b)^2 + 4a}}{2a}, \quad y_+ = bx_+, \tag{5}$$

and

$$x_- = \frac{-(1-b) - \sqrt{(1-b)^2 + 4a}}{2a}, \quad y_- = bx_-, \tag{6}$$

where x_+ and x_- are the roots of the polynomial $-ax^2 - (1+b)x + 1$. This is comparable to the Lorenz system which also has two equilibrium points when $\rho > 1$ (Lorenz, 1963).

Furthermore, for certain parameter values, the Hénon map appears to have a strange attractor with Cantor set like structure. For instance, for $a = 1.4$ and $b = 0.3$, the attractor appears to consist of curves folded closely on top of each other. In addition, upon magnification near the the fixed point (x_+, y_+) (see 5), it is revealed that the curves that constitute the the attractor are folded closely on top of each other in a self-similar fractal manner that bears resemblance to a Cantor set. Hence, the attractor appears to be the product of a one-dimensional manifold with a Cantor set. This is similar to the strange attractor of the Lorenz system which appears to be the product of a two-dimensional manifold with a Cantor set (Hénon, 1976).

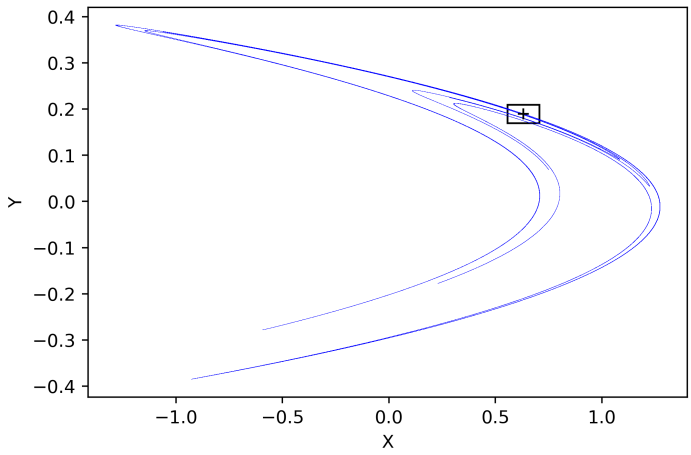

(a) $N = 10^5$

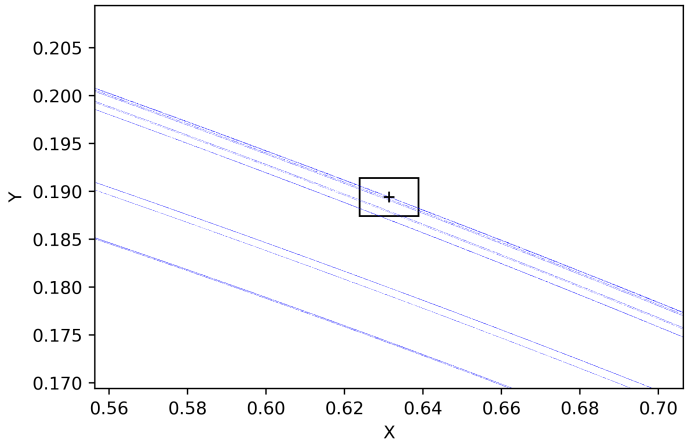

(b) $N = 10^6$

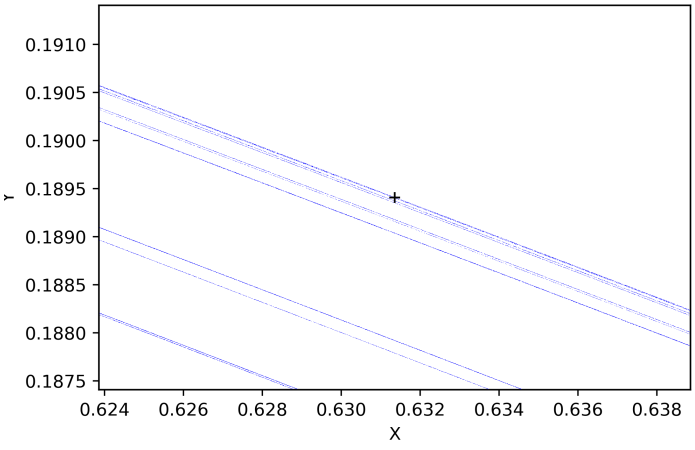

(c) $N = 10^7$

Figure 4: The figures show the last N iterations of an orbit of $N + 10^4$ iterations starting at $(x_0, y_0) = (0, 0)$ for the parameters $a = 1.4$ and $b = 0.3$. The area of (b) corresponds to the rectangle in (a), and the area of (c) corresponds to the rectangle in (b). The fixed point (x_+, y_+) (see 5) is marked with a black marker.

Comparable to the Lorenz system, the Hénon map also has a trapping region for certain parameter values, meaning a region $R \subset \mathbb{R}^2$ such that the image $H_{a,b}(R) \subset R$. For instance, the area with corners

$$\begin{aligned} (X_A, Y_A) &= (-1.33, 0.42), \qquad (X_B, Y_B) = (1.32, 0.133), \\ (X_C, Y_C) &= (1.245, -0.14), \qquad (X_D, Y_D) = (-1.06, -0.5), \end{aligned} \tag{7}$$

is a trapping region for the parameters $a = 1.4$ and $b = 0.3$ (Hénon, 1976). Figure 5 shows this region along with its image.

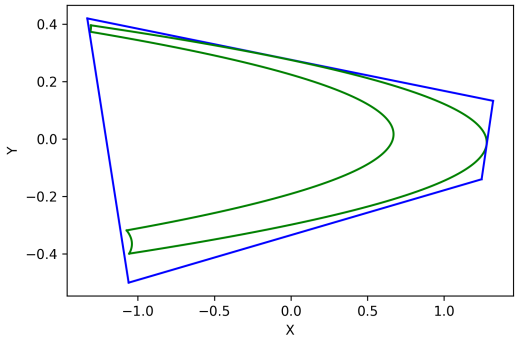

Figure 5: Trapping region with corners A, B, C, D (see 7) and the image of the region for the Hénon map with $a = 1.4$ and $b = 0.3$. The blue shape corresponds to the boundary of the trapping region and the green shape is the boundary of its image.

4 Fixed Points and Period Doubling

In this section, we discuss the fixed points of the Hénon map along with a classification of their stability in a parameter plane. We then identify curves in the parameter plane where period doubling bifurcations occur and observe numerical evidence of a period doubling cascade.

4.1 Fixed Points

As mentioned in section 3.2, the Hénon map has two fixed points (x_+, y_+) and (x_-, y_-) given by 5 and 6, respectively. These fixed points are real when $a \geq a_0 := -(1-b)^2/4$. However, since we are primarily interested in $a > 0$ and $|b| < 1$, this bound is not much of practical concern since $a_0 < 0$ for $|b| < 1$.

The characteristic polynomial of the linearization $DH_{a,b}((x, y))$ is given by

$$P(\lambda) = \lambda^2 - 2ax\lambda - b.$$

As a result, the eigenvalues at a point $(x, y) \in \mathbb{R}^2$ are given by

$$\lambda = ax \pm \sqrt{a^2x^2 + b}. \tag{8}$$

Using this, we can classify the fixed points according to their stability using definition 2.7. Figure 6 shows such a classification of the fixed points in a parameter plane. For the parameter values where the fixed point (x_+, y_+) is real, it is always a saddle. The fixed point (x_+, y_+) is an attracting fixed point for a certain region with $a \geq a_0$ and is a saddle for a region after some curve.

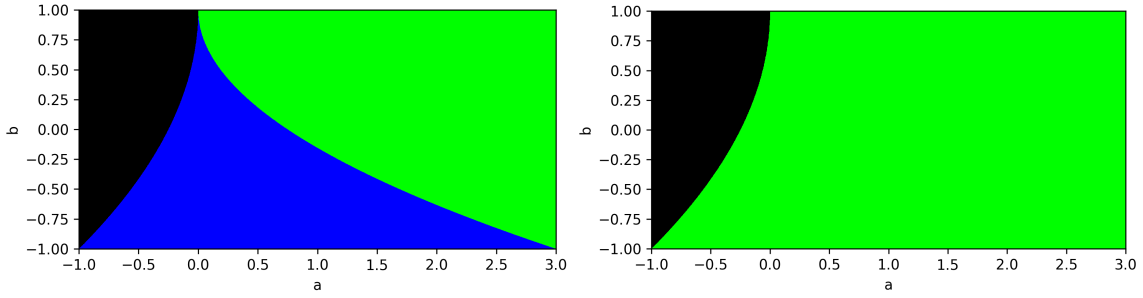

(a) Fixed point (x_+, y_+)

(b) Fixed point (x_-, y_-)

Figure 6: Classification of the fixed points (x_+, y_+) and (x_-, y_-) in a parameter plane $-1 < a < 3$ and $|b| < 1$. The black shaded area is where the fixed point is not real, blue is used when the fixed point is attracting, and green means the fixed point is a saddle point.

Upon substitution of (x_+, y_+) in 8 and solving for hyperbolic points, it is observed that (x_+, y_+) is hyperbolic for $a = -(1-b)^2/4$ and $a = 3(1-b)^2/4$. The former is a_0, which we identified as the lower bound such that the fixed points are real, and the latter is the point where (x_+, y_+) undergoes a bifurcation and goes from an attracting point to a saddle point. For simplicity, we define $a_1 = 3(1-b)^2/4$. The following proposition summarizes these results.

Proposition 4.1. *The Hénon map $H_{a,b}$ has no real fixed points for $a < -(1-b)^2/3$ and two real fixed points given by (x_+, y_+) and (x_-, y_-) for $a \geq -(1-b)^2/4$. The fixed point (x_+, y_+) is an attracting fixed point for $-(1-b)^2/4 < a < 3(1-b)^2/4$ and a saddle for $a > 3(1-b)^2/4$. The fixed point (x_-, y_-) is a saddle for all $a > -(1-b)^2/4$.*

4.2 Period Doubling

Interestingly, at $a = a_1 = 3(1-b)^2/4$ where the fixed point (x_+, y_+) goes from an attracting fixed point to a saddle fixed point, we also see the first periodic orbit of period 2 emerge. We can find these period-2 points by solving for fixed point of $H_{a,b}^2$, i.e., points (x, y) such that

$$(x, y) = H_{a,b}^2(x, y) = \left(-a(-ax^2 + y + 1)^2 + bx + 1, -bax^2 + by + b\right).$$

From the y-coordinate, we see that

$$y = \frac{b - abx^2}{1 - b}, \tag{9}$$

which upon substituting in the x-coordinate shows that fixed points of the x-coordinate are the roots of the polynomial

$$P(x) := -a^3x^4 + 2a^2x^2 - (1-b)^3x + (1-b)^2 - a.$$

Now, since the fixed points of $H_{a,b}$ are also fixed points of $H_{a,b}^2$, we know that the x-coordinate of the fixed points of $H_{a,b}$ are also roots of $P(x)$. Hence, this shows that $P(x) = Q(x)R(x)$ with $Q(x) = -ax^2 - (1-b)x + 1$, the polynomial that has the fixed points of $H_{a,b}$ as its roots, and R some degree-2 polynomial. Using polynomial long division, we see that

$$R(x) = a^2x^2 - (1-b)ax + (1-b)^2 - a.$$

Then solving for the roots of R and substituting this in the y-coordinate 9, we get that the other two fixed points of $H_{a,b}^2$ are

$$x_{2,+} = \frac{(1-b) + \sqrt{4a - 3(1-b)^2}}{2a}, \quad y_{2,+} = \frac{b - abx_{2,+}^2}{1-b}, \tag{10}$$

and

$$x_{2,-} = \frac{(1-b) - \sqrt{4a - 3(1-b)^2}}{2a}, \quad y_{2,-} = \frac{b - abx_{2,-}^2}{1-b}, \tag{11}$$

which are real for $a \geq a_1$ and coincide with (x_+, y_+) when $a = a_1$.

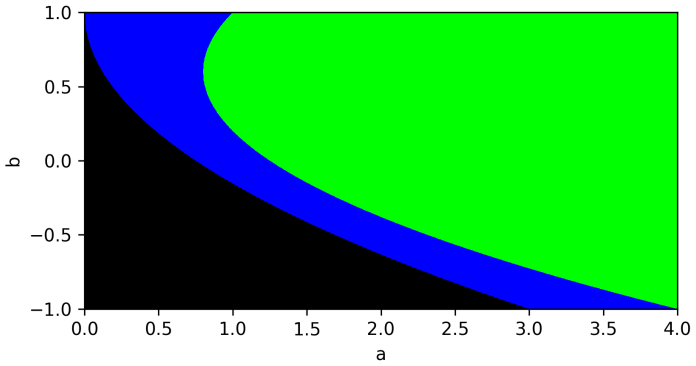

Figure 7: Stability of the fixed points $(x_{2,\pm}, y_{2,\pm})$ of $H_{a,b}^2$ in a parameter plane with $0 < a < 4$ and $|b| < 1$. The black shaded area is where the fixed point is not real, blue is used when the fixed point is attracting, and green means the fixed point is a saddle point.

Also, since $H_{a,b}(x_{2,+}, y_{2,+}) = (x_{2,-}, y_{2,-})$ and vice versa, they form a period two cycle of $H_{a,b}$. Then, as a result of 2.8, these have the same stability as fixed point of $H^2_{a,b}$ and period-2 points of $H_{a,b}$. Then, as shown in figure 7, these are attracting fixed points of $H^2_{a,b}$ for some interval $a > a_1$ and, hence, form an attracting period-2 cycle of $H_{a,b}$. Therefore, we see a period doubling bifurcation of $H_{a,b}$ at $a = a_1$.

Proposition 4.2. *At $a = a_1 := 3(1-b)^2/4$, the map $H_{a,b}$ undergoes a period doubling bifurcation, where*

- *the fixed point (x_+, y_+) is attracting for $a < a_1$;*
- *for $a \geq a_1$, a period-2 cycle emerges consisting of $(x_{2,-}, y_{2,-})$ and $(x_{2,+}, y_{2,+})$ that are equal and coincide with (x_+, y_+) at $a = a_1$;*
- *for $a > a_1$, the period-2 cycle consisting of $(x_{2,-}, y_{2,-})$ and $(x_{2,+}, y_{2,+})$ is attracting and (x_+, y_+) is no longer attracting.*

From figure 7, it also becomes evident that the period-2 cycle is only attracting for a certain region with $a \geq a_1$ and becomes a saddle later on. Solving for the hyperbolic points of $DH^2_{a,b}(x_+, y_+)$ and $DH^2_{a,b}(x_-, y_-)$ shows that the curve where this occurs is given by $a_2 := (5b^2 - 6b + 5)/4$, so that the period 2 cycle is attracting for $a_1 < a < a_2$ and a saddle for $a > a_2$. For $a > a_2$, we also see a period-4 cycle emerge upon numerical investigation, which hints at another period doubling bifurcation at $a = a_2$ and, consequently, a period doubling cascade as a increases.

Figure 8 provides further evidence of such a period doubling cascade occurring for a fixed parameter $b = 0.2$. In figure 8 only the x coordinate is shown since $y_n = bx_{n-1}$, i.e., the last thousand y-coordinates would look almost identical, except for 1 point each, to a scaled version of the last thousand x-coordinates. In addition, the respective distance of the a parameter values for which consecutive period doubling bifurcations occur also appear to be decreasing. This pattern appears to continue until, eventually, the period starts doubling erratically in a small neighbourhood approximately before $a \approx 1.149$, which can be seen from figure 9 and figure 10. After this point, the periods, if they exist, appear unidentifiable and the complexity exhibited hints at chaos. In fact, a period doubling cascade is a common route in which system become chaotic (Alligood et al., 1996).

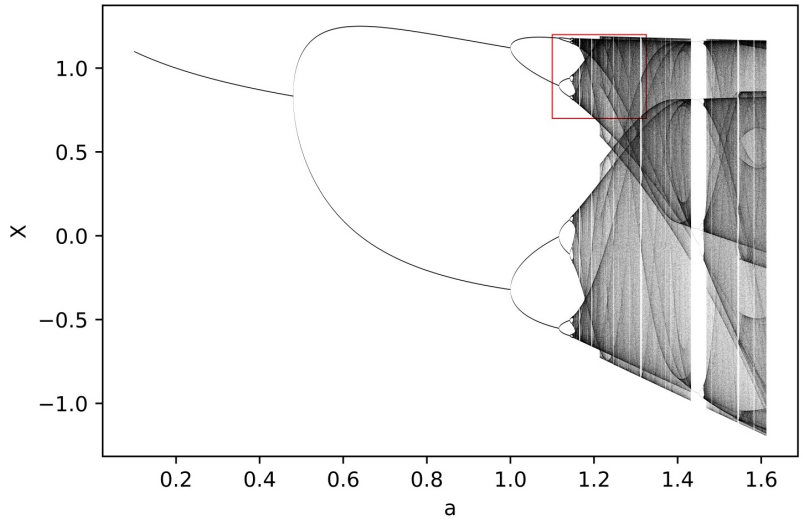

Figure 8: The x-coordinate of the last 10^3 iterations of an orbit of 10^4 iterations with $(x_0, y_0) = (0, 0)$, provided the orbit did not diverge, with $b = 0.2$, $0.1 < a < 1.7$ and stepsize $\Delta a = 10^{-4}$.

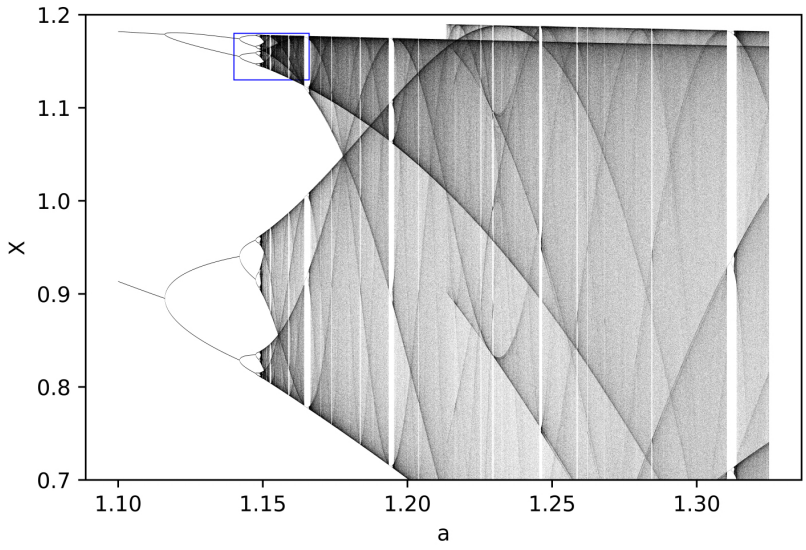

Figure 9: The x-coordinate of the last 10^3 iterations of an orbit of 10^4 iterations for $(x_0, y_0) = (0, 0)$ in the range $0.7 < x < 1.3$, provided the orbit did not diverge, with $b = 0.2$, $1.1 < a < 1.325$ and step size $\Delta a = 10^{-5}$. This corresponds to the enclosed area of the red rectangle in 8.

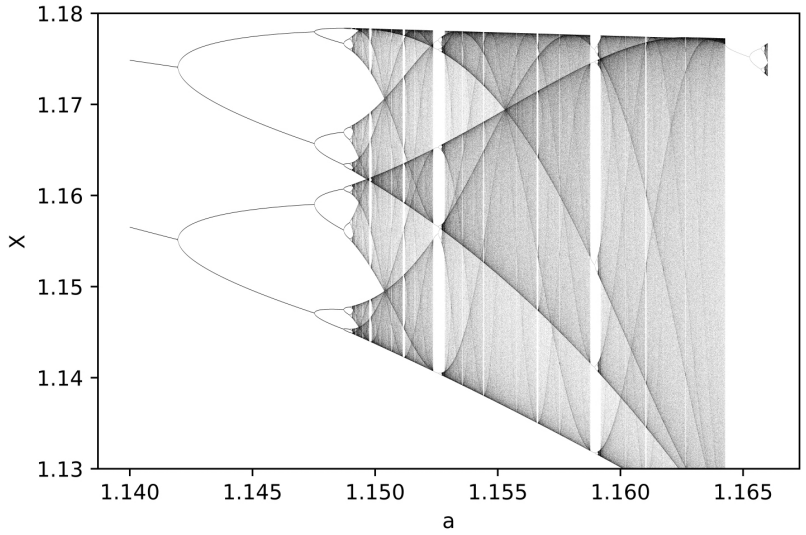

Figure 10: The x-coordinate of the last 10^3 iterations of an orbit of 10^4 iterations for $(x_0, y_0) = (0, 0)$ in the range $1.13 < x < 1.18$, provided the orbit did not diverge, with $b = 0.2$, $1.140 < a < 1.167$ and step size $\Delta a = 10^{-6}$. This corresponds to the enclosed area of the blue rectangle in 9.

Interestingly, in the region where the behaviour appears chaotic, there are also certain intervals where the systems appears to return to a periodic cycle only to return to chaotic behaviour after another period doubling cascade. This behaviour is quite similar to that of the family of one-dimensional quadratic maps, of which a famous representative is the logistic map defined by the recurrence

$$x_{n+1} = rx_n(1 - x_n) \text{ with } r > 0,$$

which is known to be chaotic for certain parameter values (Alligood et al., 1996). In addition, for the Hénon map, which is a two-dimensional quadratic map, we see that the dynamics of the x-component reduce to the recurrence

$$x_{n+1} = 1 - ax_n^2 + by_n = 1 - ax_n^2 + bx_{n-1},$$

and that whenever $b = 0$, this reduces to the dynamics of

$$F_a(x) = 1 - ax^2, \tag{12}$$

which is also a one-dimensional quadratic map. This map has been the subject of an article titled *On iterations of* $1 - ax^2$ *on* $(-1, 1)$ (Benedicks & Carleson, 1985), where this map is investigated for parameter values $0 < a < 2$. In this article, among many other things, it is shown that there exists some subset $\Delta \subset (0, 2)$, with positive Lebesgue measure, where the map has no attracting periodic orbits for $a \in \Delta$.

Theorem 4.3. *Define* $F_a : (-1, 1) \to (-1, 1)$ *by* $F_a(x) = 1 - ax^2$*, then there exists a set* $\Delta \subset (0, 2)$ *of positive Lebesgue measure such that* F_a *has no attracting periodic cycle for all* $a \in \Delta$ *(Benedicks & Carleson, 1985).*

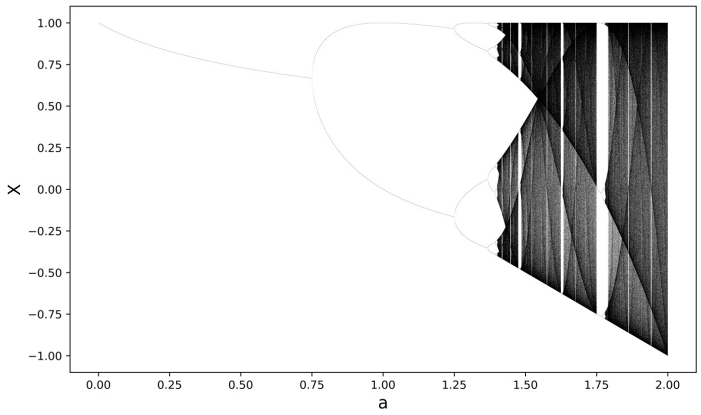

Figure 11: The last 10^3 iterations of an orbit of 10^4 iterations of $F_a(x) = 1 - ax^2$ with $x_0 = 0$ for $0 < a < 2$ and stepsize $\Delta a = 10^{-4}$.

Figure 11 also shows numerical support for this theorem since it appears that the region where the system is not attracted to a periodic cycle, which would contain Δ, has positive Lebesgue measure.

In fact, the main theorem presented in Benedicks and Carleson, 1985 is far stronger than theorem 4.3. Namely, in this paper it is also shown that there exists some $\Delta \subset (0, 2)$ of positive one-dimensional Lebesgue measure such that the dynamics of $F_a(x) = 1 - ax^2$ are chaotic for all $a \in \Delta$. Here, it should be noted that we have yet to define the type of chaos that this refers to, which is done in section 5.2, and that this is not necessarily the same type of chaos as Devaney's topological chaos introduced in the preliminaries.

The similarity of figure 11 to figure 8 might also suggest that for small $|b|$, the Hénon map, when considered as the recurrence $x_{n+1} = 1 - ax_n^2 + bx_{n+1}$, can be thought of as a perturbation of the

system defined by $F_a(x) = 1 - ax^2$. This approach to the Hénon map, by viewing it as a perturbation of $F_a(x) = 1 - ax^2$ for small values of $|b|$, is in fact what was used to derive, arguably, the most well-known results for the Hénon map proven by means of rigorous analysis in Benedicks and Carleson, 1991. In many ways, the work presented in Benedicks and Carleson, 1991 builds on the results of Benedicks and Carleson, 1985 for the map $F_a(x) = 1 - ax^2$. In section 6.2, the main theorem of Benedicks and Carleson, 1991 is discussed in further detail.

Now, to further investigate the region where the Hénon map appears to exhibits chaotic behaviour, the concept of Lyapunov exponents is useful. The next section provides a brief introduction to Lyapunov exponents along with a numerical computation of the Lyapunov exponents of the Hénon map for a set of parameters.

5 Lyapunov Exponents

The concept of Lyapunov exponents was, as the name suggests, originally thought of by Aleksandr Lyapunov in his PhD thesis *The General Problem of the Stability of Motion* (Lyapunov, 1892). In addition, in his thesis, one of the first definitions of the stability of trajectories of dynamical systems was given alongside the idea of Lyapunov functions.

Definition 5.1 (Lyapunov stable)**.** *Let $(\mathbb{R}^n, \phi, T)$ be a dynamical system. A trajectory $\phi(x_0, t)$ is stable if for any $\epsilon > 0$ there exists a $\delta > 0$ such that $||\phi(x_0, t) - \phi(x, t)|| < \epsilon$ for all $t \geq 0$ whenever $x \in B(x_0; \delta)$. A stable trajectory $\phi(x_0, t)$ is asymptotically stable if there exists a $\delta > 0$ such that $||\phi(x_0, t) - \phi(x, t)|| \to 0$ as $t \to \infty$ whenever $x \in B(x_0; \delta)$.*

Now, where the definition of Lyapunov stable and Lyapunov asymptotically stable allows for a characterization of trajectories based on whether neighbouring trajectories stay sufficiently close or whether neighbouring trajectories get attracted to it, it does not precisely quantify to what extent they do so. Then, as a way of quantifying the exponential rate of which a particular perturbation to a trajectory grows in distance to it, Lyapunov proposed the concept of characteristics exponents. Loosely speaking, given a perturbation to a trajectory, where $\delta(t)$ measures the distance over time, which is assumed to approximately grow in an exponential manner, the characteristic number λ_c is such that $\delta(t)e^{\lambda_c t}$ neither diverges to infinity nor converges to zero (Pikovsky & Politi, 2016).

However, nowadays they are usually defined as the value that approximately measures the rate of exponential growth of the distance, which would corresponds to $-\lambda_c$ if λ_c is the characteristic number as defined by Lyapunov. More precisely, using the notation of the paragraph above, the Lyapunov exponent is the number λ such that $\delta(t) \approx \delta(0)e^{\lambda t}$ (Pikovsky & Politi, 2016).

5.1 Oseledets' Multiplicative Ergodic Theorem

While Lyapunov's original definition of characteristic exponents provides a useful intuition and motivation for the use of such exponents, it fails to provide any direct method of computing them and it does not guarantee that they exits. As a result, we do not define them as such. That being said, for discrete dynamical systems defined by iterated C^1 maps, we can obtain similar numbers by relying on the fact that, locally, the map is well approximated by its linearization.

Namely, suppose $F : U \to U$ where $U \subset \mathbb{R}^n$ is some domain and F is C^1. Then, a small circle centered at $x \in U$ is mapped to an ellipsoid centered at $F(x)$ if we approximate F with the linearization DF_x, provided DF_x is nonsingular. In particular, the circle's center x is mapped to $F(x)$ and its semi-axes are stretched or contracted along some of its directions. Moreover, when DF_x is diagonalizable, this stretching effect along with the semi-axes that it occurs is characterized by the eigenvalues and corresponding eigenvectors of DF_x. Similarly, the eigenvalues and eigenvectors of DF_x^N give an approximation to how nearby points to x are mapped and the expansion behaviour of the system. Figure 12 presents an illustrative example of how a circle is mapped to an ellipse by the linearization of a C^1 map of the plane.

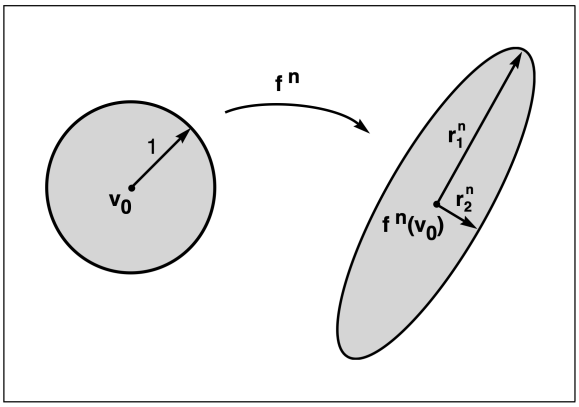

Figure 12: Example of how, with $f : \mathbb{R}^2 \to \mathbb{R}^2$ a C^1 map, f^n maps a disk centered at v_0 to an ellipsoid centered at $f^n(v_0)$ when approximating f with its linearization $(Df^n)_{v_0}$. Figure taken from Alligood et al., 1996.

Now suppose, for illustrative purposes, we simplify the case further and assume that the linearization DF_x is equal to a constant matrix A for all $x \in U$. Suppose also that all eigenvalues of A are distinct and satisfy $|\lambda_1| > \ldots > |\lambda_n| > 0$ with respective eigenvectors $v_1, \ldots, v_n$. Then, for a small $v \in \mathbb{R}^n$ with $v = \sum_{i=1}^n c_i v_i$, we have

$$F^N(x+v) - F^N(x) \approx (DF^N)_x(v) = DF_{F^{N-1}(x)} \circ \ldots \circ DF_x(v) = A^N v = \sum_{i=1}^n c_i A^N v_i = \sum_{i=1}^n c_i \lambda_i^N v_i,$$

where, assuming $c_1 \neq 0$, the right-hand sides tends to the direction corresponding to the dominant eigenvalue λ_1, and thus for sufficiently large N can be approximated with

$$||F^N(x+v) - F^N(x)|| \approx ||c_1 \lambda_1^N v_1|| = e^{N \log |\lambda_1|} ||c_1 v_1|| \propto e^{N \log |\lambda_1|} ||v||.$$

Now adopting the notation $\delta(N) = F^N(x+v) - F^N(v)$, where $\delta(0) = v$, we see that this translates to

$$||\delta(N)|| \propto e^{N \log |\lambda_1|} ||\delta(0)||,$$

which would imply that $\delta(N) e^{-N \log |\lambda_1|}$ neither diverges to infinity nor converges to zero as $N \to \infty$. As a result, we see that $-\log |\lambda_i|$ corresponds to Lyapunov's definition of the characteristic exponent of x in the direction of v and, hence, $\log |\lambda_i|$ would be the Lyapunov exponent at x in the direction of v. In particular, when k is the smallest index such that $c_k \neq 0$, then $\log |\lambda_k|$ would be the Lyapunov exponent at x in the direction of v. So, we see that the set of possible Lyapunov exponents at x is given by $\log |\lambda_i|$, where λ_i are the eigenvalues of A. Moreover, when $V_k = \text{span}\{v_j : k \leq j \leq n\}$ and $V_{n+1} = \{0\}$, we see that the Lyapunov exponent at x in the direction of v is $\log |\lambda_k|$ whenever $v \in V_k \setminus V_{k+1}$.

It should be noted that this example is indeed an oversimplification. However, as it turns out, it provides some useful intuition for the multiplicative ergodic theorem, which is an important result regarding the existence of Lyapunov exponents that was proven in 1968 by Valery Oseledets (Oseledets, 1968).

Theorem 5.2 (Oseledets' Multiplicative Ergodic Theorem)**.** *Let $F : U \to U$ be C^1 where $U \subset \mathbb{R}^n$ is some domain. In addition, suppose F defines an ergodic probability preserving system and that DF_x satisfies some further regularity properties. Then, for almost all $x \in U$, meaning that the complement of this set has Lebesgue measure zero, there exists numbers*

$$\lambda_1 > \cdots > \lambda_k, \tag{13}$$

and subspaces

$$T_xU \cong \mathbb{R}^n = V^1 \supsetneq V^2 \supsetneq \cdots \supsetneq V^k \supsetneq V^{k+1} = \{0\}$$

such that for all $v \in V^i \setminus V^{i+1}$, we have

$$\lim_{N\to\infty} \frac{1}{N} \log ||(DF^N)_x v|| = \lambda_i. \tag{14}$$

Furthermore, the numbers λ_i are constant along the orbit of x defined by F.

The formulation of the theorem is a weaker result than the original theorem and an adaptation of the formulation presented in (Filip, 2017).

Technicalities regarding the the probability preserving nature of the system and assumptions on DF_x have intentionally been omitted. A more formal treatment of the explicit assumptions and a proof of the theorem requires concepts from ergodic theory. Given the fact that this would require quite a few preliminaries, especially from measure theory, we do not cover it. Instead, for a relatively brief overview of the definitions for the formal presentation of theorem 14 along with a proof of the theorem, we refer the reader to Filip, 2017. For a more extensive and detailed discussion of the aforementioned, we refer the the reader to Viana, 2014.

As a result of theorem 5.2 and in line with the previous discussion regarding the relation of Lyapunov exponents and 14, we formulate a more practical definition of Lyapunov exponents, which also accounts for the fact that the numbers λ_i are constant along orbits.

Definition 5.3 (Lyapunov Exponents)**.** *Let $F : U \to U$ where $U \subset \mathbb{R}^n$ is some domain and F is C^1. For $x \in U$ and $v \in \mathbb{R}^n$ the corresponding number λ such that*

$$\lambda = \lim_{N\to\infty} \frac{1}{N} \log ||(DF^N)_x v||, \tag{15}$$

provided the limit exists, is the Lyapunov exponent of x in the direction of v. The set of all possible Lyapunov exponents for an orbit defined by $x \in U$ is called the Lyapunov spectrum of this orbit and coincides with the set of numbers $\lambda_1 > \cdots > \lambda_k$ given by 13. For purposes of simplicity, we often denote the Lyapunov spectrum as $\lambda_1 \geq \cdots \geq \lambda_n$, where, in the notation of theorem 14, the i-th number of 13 is repeated $\dim V^i - \dim V^{i+1}$ *many times.*

Defining Lyapunov exponents as such, i.e., we condition on whether the limit given by 15 exists, has the benefit that it is easier to work with numerically, and that we do not have to check whether the conditions of theorem 14 are satisfied. Hence, the fact that some of the conditions of theorem 5.2 have been omitted, does not cause many problems for our purposes.

Despite formulating the definition as such, we see that this definition of Lyapunov exponents corresponds rather well with Lyapunov's idea of characteristics exponents. Namely, for $x \in U$ and some sufficiently small perturbation $x + v \in U$ with corresponding Lyapunov exponent λ, we see that for sufficiently large N

$$||F^N(x + v) - F^N(x)|| \approx ||(DF^N)_x v|| \propto e^{N\lambda}, \tag{16}$$

meaning that they indeed provide a good classification of the rate of exponential separation of nearby trajectories, which was originally intended by Lyapunov. In this way, the Lyapunov exponents provide a way to classify the system's sensitivity to initial conditions along orbits.

Also, as a consequence of the multiplicative ergodic theorem, the largest Lyapunov exponents λ_1 of an orbit defined by $x \in U$ is in some sense the most indicative of the sensitivity of the system along orbits. Namely, since

$$\lambda_1 = \lim_{N\to\infty} \frac{1}{N} \log ||(DF^N)_x v|| \text{ for all } v \in V^1 \setminus V^2,$$

where $V^1 = \mathbb{R}^n$, and V^2 is a subspace of $\mathbb{R}^n$ of dimension strictly less than n and thus has Lebesgue measure zero as a subset of $\mathbb{R}^n$, we see that

$$\lambda_1 = \lim_{N\to\infty} \frac{1}{N} \log ||(DF^N)_x v|| \text{ for almost all } v \in \mathbb{R}^n. \tag{17}$$

Henceforth, whenever it is said that a property holds almost everywhere or for almost all, it means that the complement of this set has Lebesgue measure zero as a subset of $\mathbb{R}^n$. As a consequence of 17, whenever $v \in \mathbb{R}^n$ is some perturbation with uniform and randomly chosen direction, then the Lyapunov exponent in that direction is the largest Lyapunov exponent λ_1 with probability 1.

5.2 Classification

Besides the Lyapunov spectrum being equal for points along an orbit, it is generally also the case that the Lyapunov exponents are equal for all initial points in the basin of a attraction of a particular attractor (Parker & Chua, 1989; Pikovsky & Politi, 2016). Roughly speaking, this is due to the fact that the Lyapunov exponents along an orbit are defined as a limit along that particular orbit, which causes the transient behavior to be irrelevant. As a result, points lying in the basin of attraction of the same attractor will have the same Lyapunov spectrum since their limiting behaviour will be fairly similar.

Remark 5.4. *Suppose $F : U \to U$ is C^1 and $U \subset \mathbb{R}^n$. If $x, y \in U$ satisfy $\omega(x) = \omega(y)$ then the Lyapunov spectrum of x and y are the same. As a consequence, if Λ is an attractor and x, y are two points in its basin of attraction, then the Lyapunov spectrum of x and y are the same (Parker & Chua, 1989).*

This observation is presented in the form of a remark since there are generally exceptional cases for which they are not true. For this reason, we present this observation and the following observations in the form of remarks. Although these remarks are not fully rigorous, they are still quite accurate in the sense that the exceptional cases are rare and usually happen on sets of Lebesgue measure zero (Pikovsky & Politi, 2016; Viana, 2014). So, for the purposes of numerical investigation, these remarks are quite sound and serve as useful heuristics.

Despite not rigorously proving these remarks, we will still motivate them by providing plausibility arguments. For a more formal treatment of these observations and the proof of their rigorous analogues, we refer the reader to Viana, 2014.

Now, given the observation of remark 5.4, it follows that the Lyapunov spectrum can also be considered as a property of the attractor. In fact, it is quite indicative of the attractor type (Parker & Chua, 1989; Pikovsky & Politi, 2016). In this way, the Lyapunov spectrum of points in its basin of attraction can be used to classify the attractor type. For instance, whenever an orbit is in the basin of attraction of an attracting k-periodic cycle of F, the Lyapunov spectrum of this orbit is related to the eigenvalues of the periodic points when considering them as fixed points of F^k.

Remark 5.5. *Let $F : U \to U$ where $U \subset \mathbb{R}^n$ is some domain and F is C^1. If $x \in U$ is in the basin of attraction of an attracting k-periodic cycle and $y \in U$ is any point on that cycle, then the Lyapunov exponents along the orbit of x are $\lambda_i = \frac{1}{k} \log |m_i|$ where m_i are the eigenvalues of $(DF^k)_y$ (Parker & Chua, 1989).*

To provide some intuition, the following plausibility argument is quite useful, namely suppose $x \in U$ is in the basin of attraction of an attracting k-periodic cycle of a C^1 map $F : U \to U$ and $y \in U$ is any periodic point on that cycle. Since points lying in the same basin of attraction have the same Lyapunov exponents by remark 5.4, it follows that the Lyapunov spectrum along the orbit of x is equal to the Lyapunov spectrum along the periodic orbit of y, which x tends towards. Suppose also, for the sake of argument, that the eigenvalues $m_1, \ldots, m_n$ of $(DF^k)_y$ are real distinct and satisfy $|m_1| > \cdots > |m_n| > 0$ with eigenvectors $v_1, \ldots, v_n$.

Then, if λ is the Lyapunov exponent of y in the direction of v_i, we see that

$$\begin{aligned}
\lambda &= \lim_{N\to\infty} \frac{1}{N} \log ||(DF^N)_y v_i|| \\
&= \lim_{l\to\infty} \frac{1}{kl} \log ||(DF^{kl})_y v_i|| \\
&= \lim_{l\to\infty} \frac{1}{kl} \log ||(DF^k)_y^l v_i|| \\
&= \lim_{l\to\infty} \frac{1}{kl} \log ||m_i^l v_i|| \\
&= \lim_{l\to\infty} \frac{1}{kl} \left(l \log |m_i| + \log ||v_i||\right) \\
&= \frac{1}{k} \log |m_i|,
\end{aligned}$$

where we implicitly used that subsequences of convergent sequences tend to the same limit, the chain rule, and k-periodicity of the orbit of y. Therefore, we see that $\lambda_i = \frac{1}{k} \log |m_i|$ for $i = 1, \ldots, n$, which gives the full Lyapunov spectrum. As a reminder, the reason why the choice of periodic point on the cycle is irrelevant is because of proposition 2.8.

From this observation, we can also obtain two other useful corollary heuristics, which we again present as remarks. Namely, whenever a k-periodic cycle is attracting and y is a point on the cycle, the eigenvalues of $(DF^k)_y$ are strictly less than 1 in absolute value and, hence, all Lyapunov exponents are negative.

Remark 5.6. *Let $F : U \to U$ where $U \subset \mathbb{R}^n$ is some domain and F is C^1. If $x \in U$ is in the basin of attraction of an attracting periodic cycle then all Lyapunov exponents of the orbit of x are strictly negative.*

In addition, in the case of period-doubling bifurcations, the Lyapunov exponents also behave in a typical manner. To illustrate, suppose a C^1 map $F_a : U \to U$ now smoothly depends on a parameter a and has a period doubling bifurcation at $a = a^*$, where an k-periodic cycle is attracting for $a < a^*$, and for $a > a^*$ we see an attracting $2k$-periodic cycle emerge out of the k-periodic cycle which is no longer attracting. Now consider some $x \in U$ which lies in the basin of attraction of the k-periodic cycle for $a < a^*$ and in the basin of attraction of the $2k$-periodic cycle for $a > a^*$. Then, for both $a < a^*$ and $a > a^*$, the Lyapunov exponents of the orbit of x will be negative by remark 5.6.

In addition, as $a \uparrow a^*$, the largest Lyapunov exponent of the orbit of x will tend to 0. To see why, let y be a point on the k-periodic orbit and let m_1 be its dominant eigenvalue, meaning largest absolute value. Then, using the observation of remark 5.5, we have $\lambda_1 = \frac{1}{k} \log |m_1|$. Now, since the

k-periodic cycle is attracting for $a < a^*$, and it is no longer attracting for $a > a^*$, this implies that $|m_1| < 1$ for $a < a^*$ and $|m_1| > 1$ for $a > a^*$. As a result, since we assumed that F depends smoothly on a, we see that $|m_1| \uparrow 1$ as $a \uparrow a^*$ and, hence, this implies $\lambda_1 \uparrow 0$ as $a \uparrow a^*$. In a similar manner, we can show that $\lambda_1 \uparrow 0$ as $a \downarrow a_*$ where λ_1 now corresponds to the largest Lyapunov exponent of the attracting $2k$-periodic cycle for $a > a^*$. This observation is summarized in the following heuristic.

Remark 5.7. *Suppose $F_a : U \to U$ is a C^1 map that depends smoothly on the parameter a where $U \subset \mathbb{R}^n$ is some domain. Suppose also that at $a = a^*$ a period doubling bifurcation occurs. Then whenever $x \in U$ lies in the basin of attraction of the respective periodic cycles for both $a < a^*$ and $a > a^*$ and λ_1 is the largest Lyapunov exponent of the orbit of x, then $\lambda_1 \uparrow 0$ as $a \to a^*$.*

In fact, a largest Lyapunov exponent of zero is typical of bifurcations (Pikovsky & Politi, 2016). Also, because of 16 and 17, a largest Lyapunov exponent of zero implies that for sufficiently large N, we have

$$||F^m(x + v) - F^m(x)|| \propto 1$$

for all $m \geq N$ and for almost all $v \in \mathbb{R}^n$, meaning that

$$||F^m(x + v) - F^m(x)|| \approx C,$$

where C is some real constant, for all $m \geq N$ and for almost all $v \in \mathbb{R}^n$. For this reason, the case where the largest Lyapunov exponent is zero is also classified as an invariant circle.

Lastly, we see that a strictly positive largest Lyapunov exponent at a point x corresponds rather well with the intuitive understanding of what it means to have sensitive dependence on initial conditions at the point x, since 16 and 17 imply that almost all nearby obits will diverge from the orbit of x in an exponential manner. Similarly, in the case of sensitive dependence on initial conditions, it should be expected that the largest Lyapunov exponent is strictly positive (Broer & Takens, 2009).

For this reason, for practical purposes, a point x can be considered as having sensitive dependence on initial conditions if it has a strictly positive largest Lyapunov exponent. Now, whenever we want to use this to classify orbits as chaotic, we require a few more assumptions. For instance, the case of a positive Lyapunov exponent for some point in an open neighborhood where points diverge towards infinity does not correspond well with our intuitive understanding of chaos, since the orbits are quite predictable. The definition provided by Alligood et al., 1996, which can be attributed to James Yorke, excludes such cases.

Definition 5.8 (Yorke's definition of a chaotic orbit)**.** *Let $F : U \to U$ where $U \subset \mathbb{R}^n$ is a domain. Suppose $x \in U$ and that the orbit of x is bounded. Then the orbit of x is said to be chaotic if*

1. *F is not asymptotically periodic;*
2. *the largest Lyapunov exponent of x is strictly positive;*
3. *no Lyapunov exponent of x is equal to zero.*

Here, not asymptotically periodic means that the orbit does not tend towards a periodic orbit (Alligood et al., 1996).

The reason why the last condition is relevant is best shown with an illustrative example presented in Alligood et al., 1996. Namely, consider the map $F : \mathbb{R}^2 \to \mathbb{R}^2$ with polar coordinates given by

$$F(r, \theta) = (r^2, \theta + q),$$

where q is such that $\frac{q}{2\pi} \notin \mathbb{Q}$. It is not difficult to see that points with $r > 1$ will diverge towards infinity and that point with $r < 1$ will converge towards the origin. In addition, points with $r = 1$ will always lie on the unit circle and these orbits are not asymptotically periodic since $\frac{q}{2\pi} \notin \mathbb{Q}$. Also, since

$$(DF)_{(r,\theta)} = \begin{bmatrix} 2r & 0 \\ 0 & 1 \end{bmatrix},$$

we see that the Lyapunov exponents for points on the unit circle are $\lambda_1 = \log 2$ and $\lambda_2 = 0$, since their orbits always stay on the unit circle. However, the orbits on the unit circle behave quite predictably, since they just spiral around the origin with a constant angle q. Hence, despite the fact that such orbits have a positive Lyapunov exponent and are not asymptotically periodic, the behaviour is still quite predictable.

Then, using the definition of a chaotic orbit, a definition is given of a chaotic set and a chaotic attractor.

Definition 5.9 (Yorke's definition of a chaotic attractor)**.** *Let $F : U \to U$ where $U \subset \mathbb{R}^n$ is a domain and let $x \in U$. Then the ω-limit set $\omega(x)$ is said to be a chaotic set if there exists a $y \in \omega(x)$ such that the orbit of y is chaotic in terms of definition 5.8. In addition, an attractor Λ is said to be a chaotic attractor if Λ is a chaotic set (Alligood et al., 1996).*

It should be noted that the implied definition of an attractor here is somewhat different than that of definition 2.10. For this latter definition, it is required that there exists arbitrarily small neighbourhoods U of the attractor Λ such that $\omega(y) \subset \Lambda$ for all $y \in U$. However, Yorke's definition of an attractor is less restrictive, and more practical to work with for numerical purposes

Definition 5.10 (Yorke's definition of an Attractor)**.** *Let $F : U \to U$ where $U \subset \mathbb{R}^n$ is a domain. A ω-limit set $\omega(x)$ for $x \in U$ is an attractor, if there exists $V \subset U$ with non-zero n-dimensional Lebesgue measure such that $\omega(y) \subset \omega(x)$ for all $y \in V$ (Alligood et al., 1996).*

Using Yorke's definition of a chaotic attractor, we can then formulate a useful heuristic, which we again present as a remark. This remark is formulated in a manner that is somewhat vague but will nevertheless be quite useful for numerically classifying chaotic attractors.

Remark 5.11. *Suppose $F : U \to U$ is a diffeomorphism and $U \subset \mathbb{R}^n$ is some domain. Suppose $x \in U$ is some initial point chosen with some degree of arbitrariness. If the forward-orbit of x stays in some bounded region and the largest Lyapunov exponent of x is strictly positive with no other Lyapunov exponent of the Lyapunov spectrum of x equal to 0, then, except for rare cases, the orbit of x tends towards a chaotic attractor Λ in terms of definition 5.9*

Similar to the previous remarks, we can motivate this heuristic by a plausibility argument. Namely, suppose $F : U \to U$ is a diffeomorphism and $U \subset \mathbb{R}^n$ is some domain. Let $x \in U$ be some arbitrary initial point and suppose it satisfies the conditions above. Then, since the forward orbit of x is bounded, there exist some compact set $V \subset \mathbb{R}^n$, not necessarily contained in U, such that $F^m(x) \in V$ for all $m \geq 0$. Hence, by the Bolzano-Weierstrass property, there exists some $\omega(x) \subset V$, nonempty. In addition, since $x \in U$ is assumed to be chosen in an arbitrary manner, we can classify $\omega(x)$ as an attractor in terms of definition 5.10 with a high degree of certainty. Namely, the fact that x is somewhat arbitrary implies that the set with this ω-limit set likely has positive Lebesgue measure.

In addition, we can choose some $y \in \omega(x)$ such that the Lyapunov spectrum of y is the same as the Lyapunov spectrum of x by remark 5.4. Then, the fact that the largest Lyapunov exponent is strictly positive implies that $\omega(x)$ is not an attracting periodic cycle by remark 5.6. Also, because F is a diffeomorphism, this implies with a high degree of certainty that $\omega(x)$ is not a periodic cycle of

saddle type, since such cycles only attract nearby orbits along their local stable manifold of Lebesgue measure zero (see section 6.2). Hence, with a high degree of certainty, we can classify the orbit of y as chaotic by definition 5.8, since the Lyapunov spectrum has a strictly positive largest Lyapunov exponent, no other Lyapunov exponent is zero, and the orbit of y is not asymptotically periodic. Therefore, the attractor $\omega(x)$ contains a chaotic orbit, which by definition 5.9 implies that $\omega(x)$ is a chaotic attractor.

5.3 Lyapunov exponents of the Hénon map

For the computation of the Lyapunov exponents, we relied on the algorithm developed by Benettin et al., 1980 that uses the Gram-Schmidt orthonormalization procedure. For the details of this algorithm along with a sketch of the derivation, we refer the reader to the appendix A.1. For all the following figures in this section, this algorithm was used.

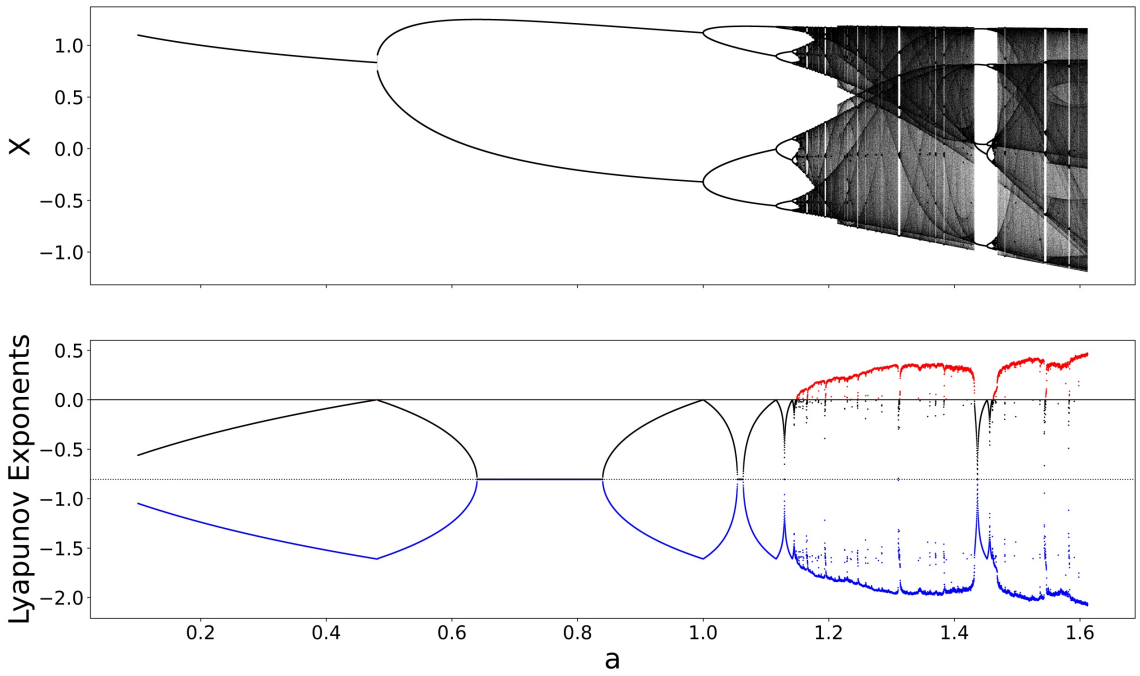

Figure 13: The above figure shows the last 10^3 iterations of an orbit of $10^4 + 10^3$ iterations, provided the orbit did not diverge, and the figure below shows the Lyapunov exponents for these orbits. The largest Lyapunov exponent λ_1 is marked black if $\lambda_1 < 0$ and red if $\lambda_1 > 0$. The other Lyapunov exponent λ_2 is marked blue. The range of a values is $0.1 < a < 1.7$ with stepsize $\Delta a = 10^{-4}$ and $b = 0.2$. The dotted line in the Lyapunov exponents figure corresponds to $\lambda = \frac{1}{2}\log(0.2)$. The initial point of this orbit is chosen in close proximity to (x_+, y_+) (see 5).

Figure 13 illustrates the same scenario of figure 8 where figure 13 now also shows the Lyapunov exponents. From figure 13, we see that both Lyapunov exponents are indeed observed to be negative for the parameters where the orbit tends to a periodic cycle. This is as predicted by remark 5.6.

Notice also that at values $a = a^*$ where a period doubling bifurcation occurs, we observe that $\lambda_1 \uparrow 0$ as $a \to a^*$ and that $\lambda_1 = 0$ at $a = a^*$, which is as predicted by remark 5.7. Also, for the regions after the period doubling cascade where the systems appears to exhibits aperiodic and erratic behaviour, we observe a positive largest Lyapunov exponents. By remark 5.11, this can be

considered as empirical evidence of chaos and a chaotic attractor in terms of definition 5.8 and definition 5.9. For values of $a > 1.622...$ the orbits diverged towards infinity and no attractor was detected.

In addition, in figure 13, we see that that the largest Lyapunov exponents λ_1 appears to be the reflection of the smaller Lyapunov exponent λ_2 about the line $\lambda = \frac{1}{2}\log(0.2)$. As it turns out, this is due to the fact that for maps with constant determinant the Lyapunov exponents satisfy a relation with respect to that determinant.

Proposition 5.12. *Let $F : U \to U$ be C^1 with a $U \subset \mathbb{R}^n$ a domain. Suppose that $\det(DF_x) = c$ for all $x \in U$ where c is a nonzero constant. If $\lambda_1 \geq \cdots \geq \lambda_n$ are the Lyapunov exponents of $x \in U$, then*

$$\log(|c|) = \sum_{k=1}^{n} \lambda_i.$$

This result is proven in Viana, 2014 and follows from the fact that the sum of the Lyapunov exponents measures the rate of volume contraction/expansion along an orbit. Although we do not give a proof of this statement, in section 6.1.2 and the appendix A.1, a plausibility argument is presented between the relation of the sum of the Lyapunov exponents and the rate of volume contraction.

Using proposition 5.12, we can derive a useful corollary for the Hénon map.

Corollary 5.13. *Suppose $\lambda_1 \geq \lambda_2$ are the Lyapunov exponents for some $(x, y) \in \mathbb{R}^2$ of $H_{a,b}$. Then,*

$$\lambda_1 + \lambda_2 = \log(|b|),$$

and

$$\lambda_1 \geq \frac{1}{2}\log(|b|), \quad \lambda_2 \leq \frac{1}{2}\log(|b|), \tag{18}$$

which also implies that $\lambda_2 < 0$, since $|b| < 1$.

This corollary is trivial to show and follows directly from proposition 5.12 and the fact that the determinant of the linearization of $H_{a,b}$ is equal to $-b$ everywhere, which we showed in section 3.2.

From corollary 5.13, we also see that, for orbits of the Hénon map, it is not possible for both Lyapunov exponents to be positive due to the fact that the system is dissipative. The cases where an attractor of a system is observed to have more than one positive Lyapunov exponents are also sometimes referred to as hyperchaos. This term was first used by Rössler, 1979 upon observing two positive Lyapunov exponents for the flow of a four-dimensional system.

Using a similar approach as for the fixed parameter $b = 0.2$ and $0.1 < a < 1.7$, we can also classify the attractor and behavior of the system in a larger parameter plane. Figure 14 shows such a classification of the system based on Lyapunov exponents, which is also commonly referred to as a Lyapunov diagram. The meaning of the colours is given in table 1. Figure 16 shows the largest Lyapunov exponent in the same parameter plane and using the same data as the Lyapunov diagram of figure 14. The Lyapunov exponents used for these figures correspond to orbits with initial points in close proximity to (x_+, y_+) (see 5).

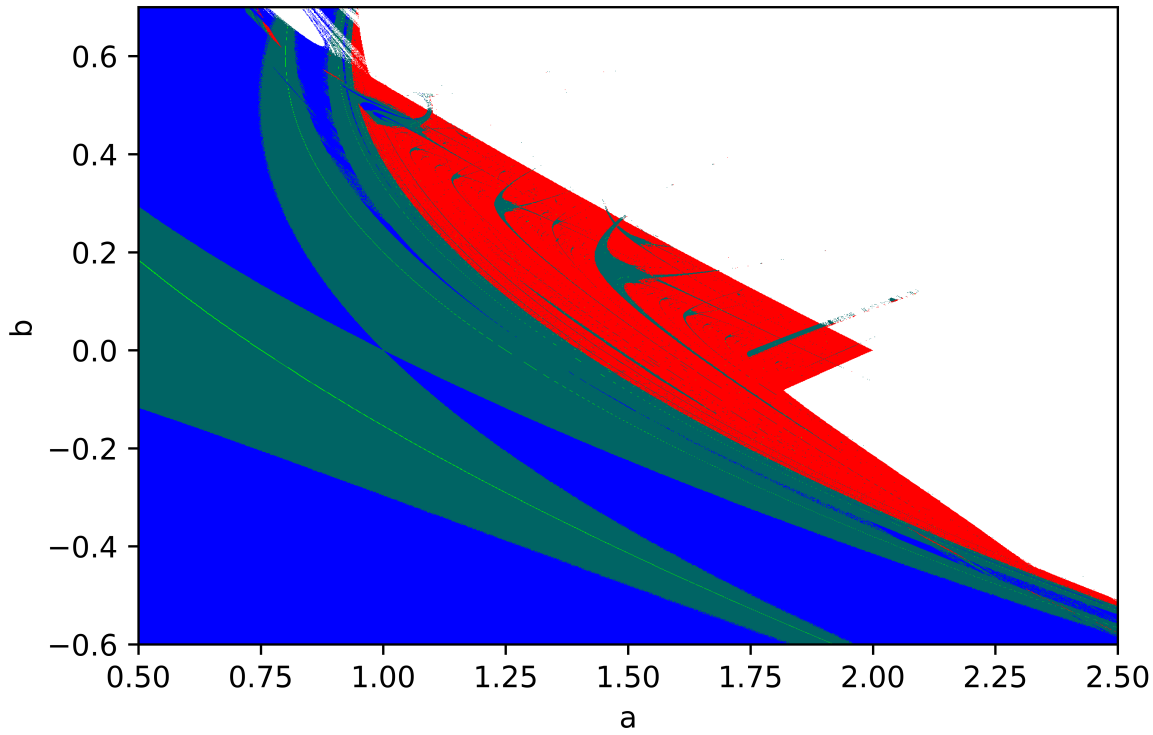

Figure 14: Lyapunov diagram of the Hénon map for the range $-0.6 < b < 0.7$ and $0.5 < a < 2.5$ with a parameter grid of 1500×1500. The colour coding is given in table 1.

Colour	Lyapunov Exponents	Attractor Type
Dark Green	$0 > \lambda_1 > \lambda_2$	Periodic cycle of node type
Blue	$0 > \lambda_1 = \lambda_2$	Periodic cycle of focus type
Light Green	$0 = \lambda_1 > \lambda_2$	Invariant circle
Red	$\lambda_1 > 0 > \lambda_2$	Chaotic Attractor
White	-	No attractor detected

Table 1: The meaning of the colours of the Lyapunov diagram of figure 14. The colour coding is inspired by Garst, 2018.

In the diagram of figure 14 and in table 1, for the cases where both Lyapunov exponents are strictly negative the attractor is classified as a periodic cycle, which is motivated by the observation of remark 5.6. In addition, according to remark 5.5, whenever an orbit tends towards an attracting n-periodic cycle the Lyapunov exponents are $\lambda_i = \frac{1}{n} \log |m_i|$ where m_i are the eigenvalues of $(DH^n_{a,b})_{(x,y)}$ with $1 > |m_1| \geq |m_2| > 0$ and where (x, y) is any point on the attracting cycle. Hence, whenever $0 > \lambda_1 = \lambda_2$ this implies that $|m_1| = |m_2|$. Also, since the eigenvalues of $(DH^n_{a,b})_{(x,y)}$ are roots of a degree two polynomial with real coefficients, whenever the eigenvalues m_1 and m_2 are complex, they are conjugate to each other and, as a result, satisfy $|m_1| = |m_2|$. So, locally the point (x, y) is an attracting fixed point of $H^n_{a,b}$ that attracts nearby orbits equally along all directions in a possibly spiraling manner, where the spiraling occurs if m_1 and m_2 are complex. Such an attracting fixed point is often characterised as an attracting fixed point of focus type and figure 15a provides an example of how a typical attracting fixed point of focus type looks like.

Through a similar line of reasoning, the case where $0 > \lambda_1 > \lambda_2$ implies that $1 > |m_1| > |m_2| > 0$ and that both m_1 and m_2 are real. If v_1 and v_2 are the respective eigenvectors of m_1 and m_2, then locally the point (x, y) is an attracting fixed point of $H^n_{a,b}$ where nearby orbits converge faster towards (x, y) along the direction of the v_2, which is the eigenvector of the smaller eigenvalue m_2, and almost all orbits will visually approach (x, y) along the direction of v_1. Such an attracting fixed is often characterised as an attracting fixed point of node type and figure 15b gives an illustrative example of how such a fixed point might look like.

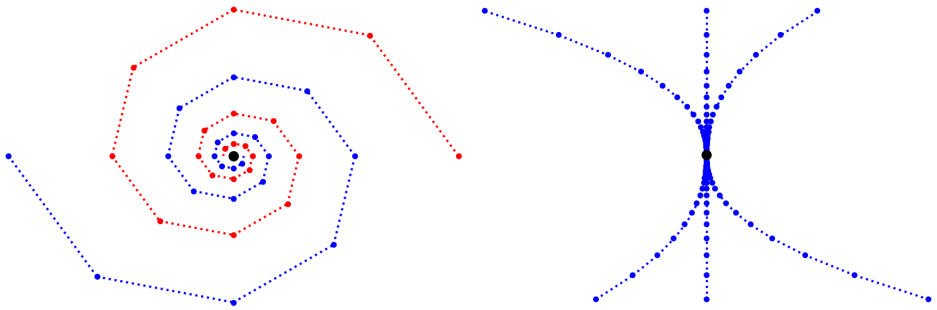

(a) Focus type fixed point (b) Node type fixed point

Figure 15: Examples of how an attracting fixed point of focus type and node type attract orbits of a discrete system. The dotted lines are used to represent consecutive iterations.

In figure 16 and table 1, the case where the largest Lyapunov exponent λ_1 is zero is classified as an invariant circle, where a motivation for this classification is provided in the previous section. For the parameter values $a = a_1 := 3(1 - b)^2/4$ and $a = a_2 := (5b^2 - 6b + 5)/4$, where period doubling bifurcations occur, we observe in figure 16 that the largest Lyapunov exponent is zero. These findings agree with the expectation presented in remark 5.7.

For the cases where the Lyapunov exponents λ_1 and λ_2 satisfy $\lambda_1 > 0$ and $\lambda_2 < 0$, the attractor is classified as a chaotic attractor by remark 5.11. In figure 14, we see numerical evidence for the presence of a chaotic attractor in some region of the parameter plane where $|b|$ is not too large and a depending on b. For purposes of simplicity, in what follows, we shall now refer to this region as the chaotic region.

From figure 14, it also seems that the parameter values in the chaotic region appear to have positive two-dimensional Lebesgue measure in the parameter plane. It is in fact proven by Benedicks and Carleson, 1991 that for small values of $b > 0$ there exists a set of a parameter values, depending on b, with positive one-dimensional Lebesgue measure such that the Hénon map has a chaotic attractor for such parameter values. We shall discuss this result in further detail in section 6.2.

In addition, in this larger region where a chaotic attractor is detected, there appear to be smaller sets, of positive two-dimensional Lebesgue measure, where the system tends to a periodic cycle. This was already observed for the parameter $b = 0.2$ in figure 13 and appears to persist throughout the parameter plane. More strongly, it is conjectured, but not yet proven, that the chaotic region is contained in the closure of the parameter values where the Hénon map has an attracting periodic cycle.

Conjecture 5.14. *The chaotic region is contained in the closure of the set of parameters where the Hénon map has an attracting periodic cycle (Benedicks & Carleson, 1991; Eckmann & Ruelle, 1985).*

If the conjecture would be true, this would also imply that the Lyapunov exponents do continuously depend on the parameters a and b, since the largest Lyapunov exponents would be strictly positive for chaotic parameter values and strictly negative for parameter values with an attracting periodic cycle. Hence, this would also explain why the Lyapunov exponents appear to be discontinuous as a function of a for fixed $b = 0.2$ in this region, which we see in figure 13.

These periodic regions in the chaotic region have also been investigated and classified according to the main periodicities that occur in them by Gallas, 1993. Here, since there are period doubling cascades in these regions, the main period k of a region is such that the periodic cycles in this region are of period $k \cdot 2^n$ for some $n \geq 0$.

Figure 17 and figure 18 provide a magnification of parts of the chaotic region observed in figure 14. Upon magnification of parts of the chaotic region, as seen in figure 17 and figure 18, we observe that these periodic regions seem to assume peculiar shapes in the parameter plane. For reasons that are hopefully clear, these regions are also referred to as shrimps and swallows (Nusse & Yorke, 1998). From figure 17 and figure 18, it also appears that these swallows and shrimps exists for even smaller scales of the parameter plane, which might hint at a fractal structure.

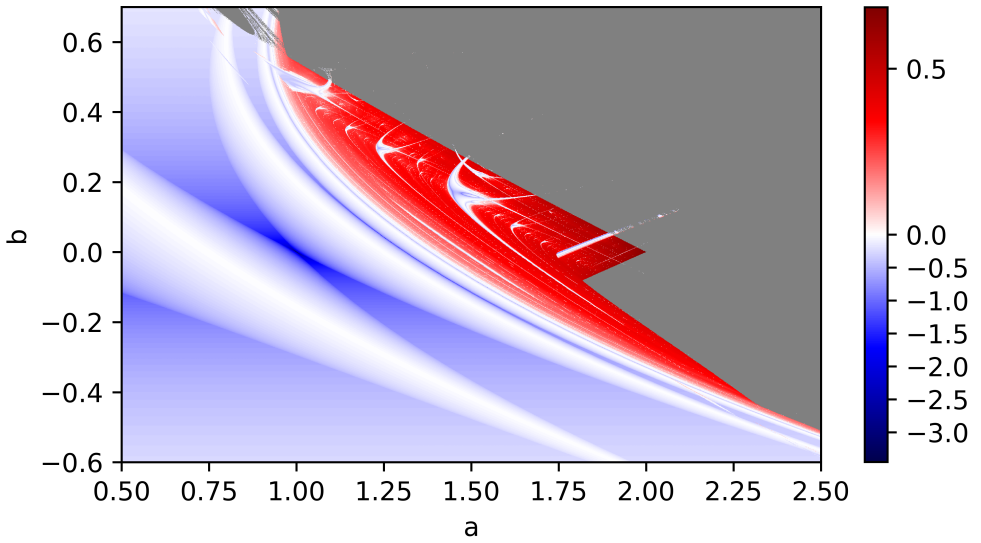

Figure 16: Classification of the system based on largest Lyapunov exponents in a parameter plane

Figure 16 shows the value of the largest Lyapunov exponent in a parameter plane for the same data used to generate the Lyapunov diagram in figure 14. This figure also provides numerical verification for a result proven in Benedicks and Carleson, 1991.

Theorem 5.15. *For all $c < \log 2$ there is a $b_0 > 0$ such that for all $b \in (0, b_0)$ there is a set $E(b)$ of positive one-dimensional Lebesgue measure such that for all $a \in E(b)$ there is a point z_0 in the attractor of $H_{a,b}$ such that*

$$||(DH_{a,b}^n)_{z_0}(0,1)|| \geq e^{cn},$$

and as a consequence $\lambda_1 \geq c$ for this orbit (Benedicks & Carleson, 1991).

Also, the largest positive Lyapunov exponent found in the 1500×1500 parameter grid of figure 16 is $\lambda_1 \approx 0.6851 < \log 2 \approx 0.6931$ for $(a, b) \approx (1.9996, -0.0003)$. So, based on this observation, it appears plausible that $\log 2$ might also be an upper bound for the largest Lyapunov exponent for the Hénon map in this parameter plane.

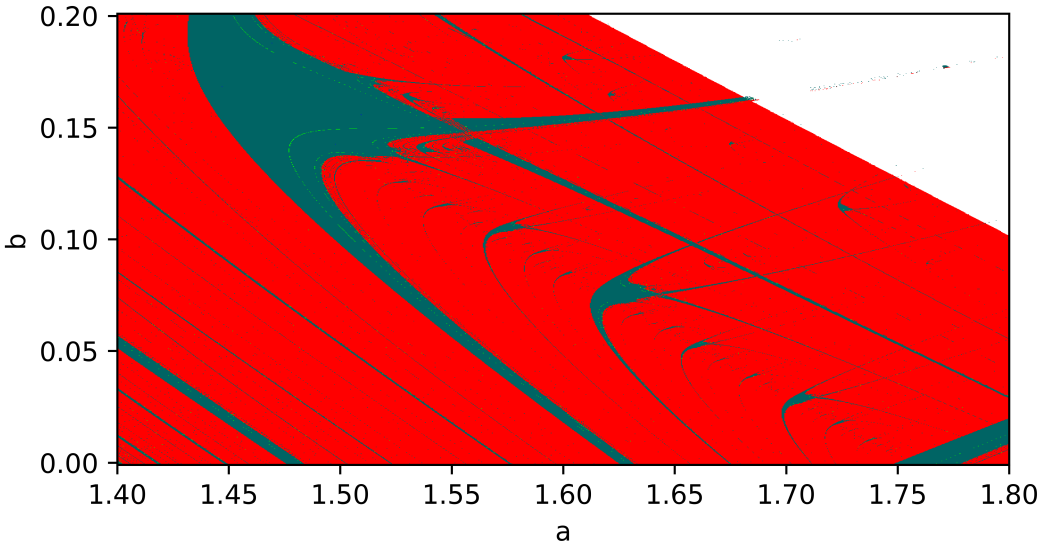

(a)

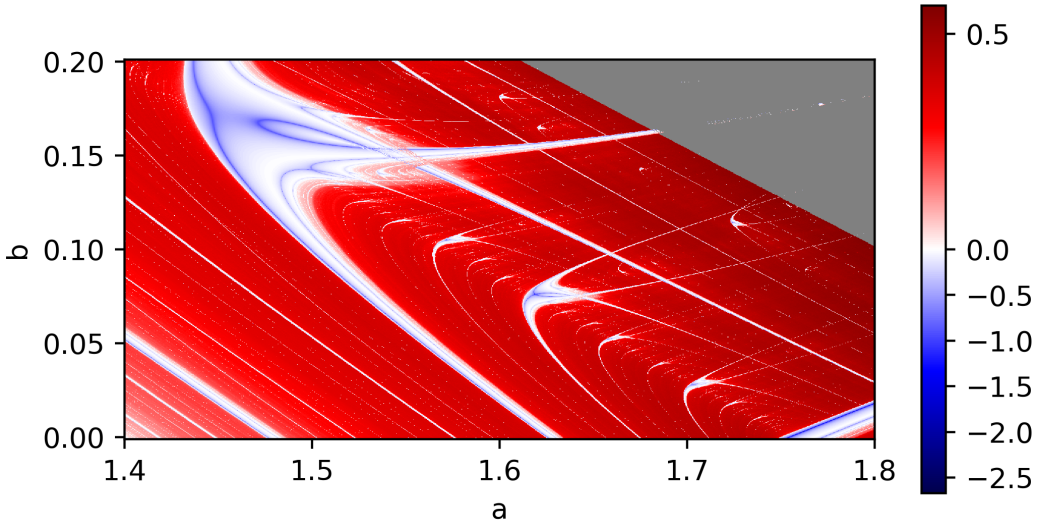

(b)

Figure 17: Lyapunov diagram and largest Lyapunov diagram for the range $0 < b < 0.2$ and $1.4 < a < 1.8$ with a 1000×1000 parameter grid. The color coding of the Lyapunov diagram is given in table 1.

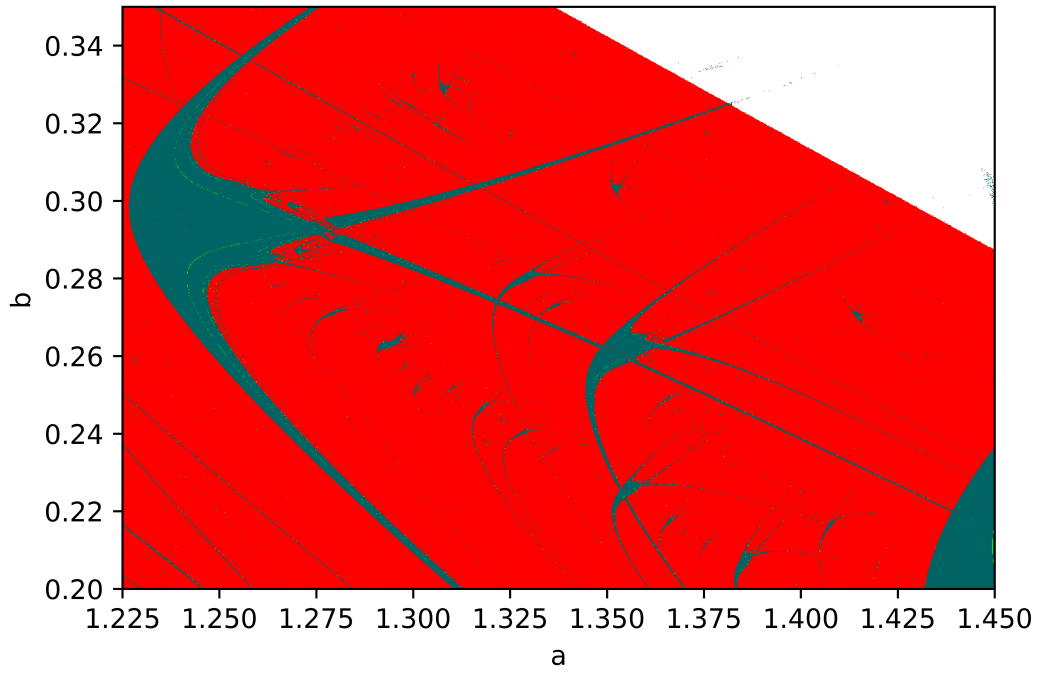

(a)

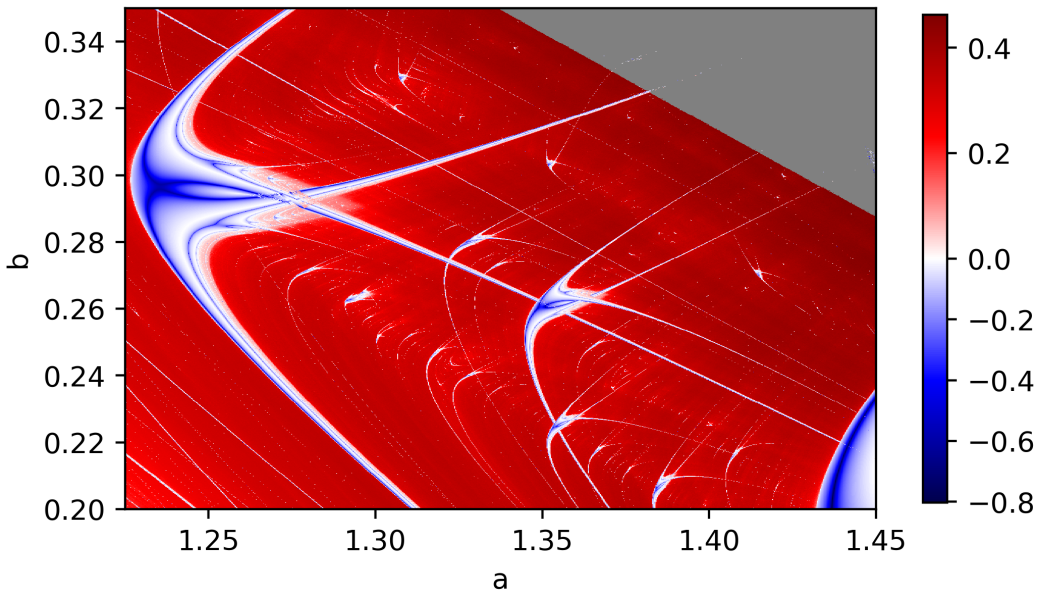

(b)

Figure 18: Lyapunov diagram and largest Lyapunov diagram for the range $0.2 < b < 0.35$ and $1.225 < a < 1.45$ with a 1000×1000 parameter grid. The color coding of the Lyapunov diagram is given in table 1.

6 Attractor

In this section, we investigate some properties of the attractor of the Hénon map. In particular, we mostly focus on the attractor for the classic parameter values $a = 1.4$ and $b = 0.3$, originally selected by Hénon, 1976. Firstly, we investigate properties relating to the fractal geometry of the attractor. We conclude this section with a discussion regarding the relation of the attractor and the unstable manifold of one of the map's saddle fixed points.

6.1 Dimension

As discussed in section 3.2 and observed in figure 4, near the fixed point (x_+, y_+), the attractor of the Hénon map appears to consist of curves folded closely on top of each other in a self-similar manner bearing familiarity to a Cantor set. As a result, the attractor seems to be a fractal that consists of the product of a one-dimensional manifold with a Cantor set. Then, in order to get a better understanding of the attractor, and of such shapes in general, we will numerically compute some it its fractal dimensions, which are dimensions that are not restricted to integers. In particular, in this section, we compute the box-counting dimension and Lyapunov dimension of the Hénon attractor along with a brief introduction to the respective dimension.

6.1.1 Capacity Dimension and Box-Counting Dimension

A simple type of fractal dimension is that of capacity dimension. This dimension is also commonly referred to as the fractal dimension. However, for clarity purposes and to avoid confusion, since we refer to multiple types of fractal dimension, we shall not use this name.

Capacity dimension can be introduced in an intuitive manner as an extension of integer dimension of simple shapes such as lines, squares, cubes, and spheres. Namely, suppose M is some smooth manifold embedded in $\mathbb{R}^n$ of dimension $1 \leq d \leq n$, necessarily an integer, and $N(\epsilon)$ is the minimum number of volume elements (boxes, balls, etc.) in $\mathbb{R}^n$ of diameter $\epsilon > 0$ required to cover M, then

$$N(\epsilon) \propto \epsilon^{-d},$$

for sufficiently small ϵ. For instance, for $\mathbb{S}^2 \subset \mathbb{R}^3$ we have

$$N(\epsilon) \propto \epsilon^{-2},$$

and for a cube $C \subset \mathbb{R}^3$, with interior, we have

$$N(\epsilon) \propto \epsilon^{-3}.$$

So, we see that for sufficiently small $\epsilon > 0$, we get

$$N(\epsilon) = k\epsilon^{-D},$$

for some real constant $k > 0$, where taking the logarithm gives

$$\log N(\epsilon) = -D \log(\epsilon) + \log(k), \tag{19}$$

which implies that

$$\lim_{\epsilon \to 0^+} -\frac{\log N(\epsilon)}{\log \epsilon)} = \lim_{\epsilon \to 0^+} -\frac{-D \log \epsilon + \log k}{\log \epsilon} = D,$$

and, as a result, motivates the following definition.

Definition 6.1 (Capacity Dimension)**.** *Suppose $A \subset \mathbb{R}^n$ is bounded and $N(\epsilon)$ is the minimum number of volume elements of $\mathbb{R}^n$ of diameter ϵ required to cover A. Then the capacity dimension D_{cap} is defined as*

$$D_{cap} = \lim_{\epsilon \to 0^+} -\frac{\log N(\epsilon)}{\log \epsilon}, \tag{20}$$

provided the limit exists (Parker & Chua, 1989).

As it turns out, defining capacity dimension as such allows for it to take on non-integer values for complex shapes such as fractals.

To give an illustrative example of such a fractal with non-integer capacity dimension, we consider the middle third Cantor set. As a brief reminder, the Cantor set $C \subset [0,1]$ is constructed by iterative removal of the open middle third of the intervals in C_n, where $C_0 = [0,1]$. For instance, the iterates are given by $C_1 = [1, 1/3] \cup [2/3, 1]$, $C_2 = [1, 1/9] \cup [2/9, 1/3] \cup [2/3, 7/9] \cup [8/9, 1]$ and, more generally, where

$$C_n = \bigcup_{a \in \{0,2\}^n} \left[\sum_{i=1}^{n} a_i 3^{-k}, \sum_{i=1}^{n} a_i 3^{-k} + 3^{-n} \right],$$

is the union of 2^n disjoint intervals of length 3^{-n} (de Snoo & Winkler, 2023). Then the Cantor set C is given as the nested intersection of the C_n's, namely

$$C = \bigcap_{n=0}^{\infty} C_n.$$

Now consider intervals of length $\epsilon = 3^{-k}$ with $k \geq 1$. We see that the number of intervals of length 3^{-k} required to cover C equals the number of intervals required to cover C_k and is equal to 2^k, since C_k consists of 2^k intervals of length 3^{-k} that are separated by a distance greater than 3^{-k}, and the fact that $C^n \subset C^k$ for $n \geq k$. Then, provided the limit given by 20 exists, which is implied by Parker and Chua, 1989, we see that

$$\begin{aligned} D_{cap} &= \lim_{\epsilon \to 0^+} -\frac{\log N(\epsilon)}{\log \epsilon} \\ &= \lim_{k \to \infty} -\frac{\log N(3^{-k})}{\log 3^{-k}} \\ &= \lim_{k \to \infty} -\frac{\log 2^k}{\log 3^{-k}} \\ &= \lim_{k \to \infty} -\frac{k \log 2}{-k \log 3} \\ &= \frac{\log 2}{\log 3} = 0.63\ldots, \end{aligned}$$

which shows that the Cantor set has non-integer dimension. So, despite the Cantor set having one-dimensional Lebesgue measure zero (de Snoo & Winkler, 2023), it still occupies some 'space' in the interval $[0,1]$ in the sense that there is no upper bound N to the minimum number of boxes such that the Cantor set can be covered with less than N intervals of length ϵ for all $\epsilon > 0$.

In fact, interpreting the capacity dimension of a set $A \subset \mathbb{R}^n$ as a measure of how it occupies space in $\mathbb{R}^n$ proves to be a rather intuitive way of thinking about the capacity dimension, albeit a

bit vague. For instance, the Cantor set does not sit in $\mathbb{R}$ as a finite collection of points, which have capacity dimension 0, nor does sit in $\mathbb{R}$ as an interval would, which have capacity dimension 1. So, the Cantor set is something more than a finite collection of points and something less than a interval in terms of how it occupies space (Parker & Chua, 1989). On the other hand, the set $\mathbb{Q} \cap [0, 1]$ has capacity dimension 1, meaning that, although it is a countable collection of points, it occupies space as if an interval would, which also makes sense since $\mathbb{Q} \cap [0, 1]$ is dense in $[0, 1]$.

The capacity dimension does present some difficulties since the minimum number of volume elements required for a given ϵ may vary for the volume element used, i.e., it might require more boxes than balls to cover a particular set (Parker & Chua, 1989). For practical purposes, this makes the capacity dimension rather difficult to compute numerically. So, instead of computing the capacity dimension of the Hénon attractor, we restrict our attention to coverings of the attractor where the volume elements are boxes. This dimension is aptly named the box-counting dimension.

Definition 6.2 (Box-Counting Dimension)**.** *Suppose $A \subset \mathbb{R}^n$ is bounded and $N(\epsilon)$ is the minimum number of boxes of $\mathbb{R}^n$ of side length ϵ required to cover A. Then the box-counting dimension D_{box} is defined as*

$$D_{box} = \lim_{\epsilon \to 0^+} -\frac{\log N(\epsilon)}{\log \epsilon}, \tag{21}$$

provided the limit exists (Parker & Chua, 1989).

In order to compute this value, we rely on the box-counting technique presented in Parker and Chua, 1989. The method relies on covering the state space with a grid of boxes of side length ϵ and counting the number of boxes that contain elements of the respective set. Then, in order to compute the box-counting dimension D_{box}, we repeat this procedure for various small $\epsilon > 0$ and compute the slope of the log-log plot of $N(\epsilon)$ and $-\log \epsilon$, where $N(\epsilon)$ is the number of boxes that contain elements of the set.

A motivation for this method is the fact that, in a similar manner as above, we see that the box-counting dimension approximately satisfies

$$\log N(\epsilon) = -D_{box} \log \epsilon + \log k, \tag{22}$$

for some real constant $k > 0$, and $\epsilon > 0$ sufficiently small. Therefore, choosing a sufficiently small ϵ and computing D_{box} as $-\log N(\epsilon)/\log \epsilon$ would still result in error term of $-\log k/\log \epsilon$. However, from 22, computing D_{box} as the slope of a least-squares linear fit of the log-log plot of $N(\epsilon)$ and $-\log \epsilon$, for various sufficiently small values of $\epsilon > 0$, would resolve this. For the interested reader, a more detailed account of this method as well the algorithm used is presented in the appendix A.2.

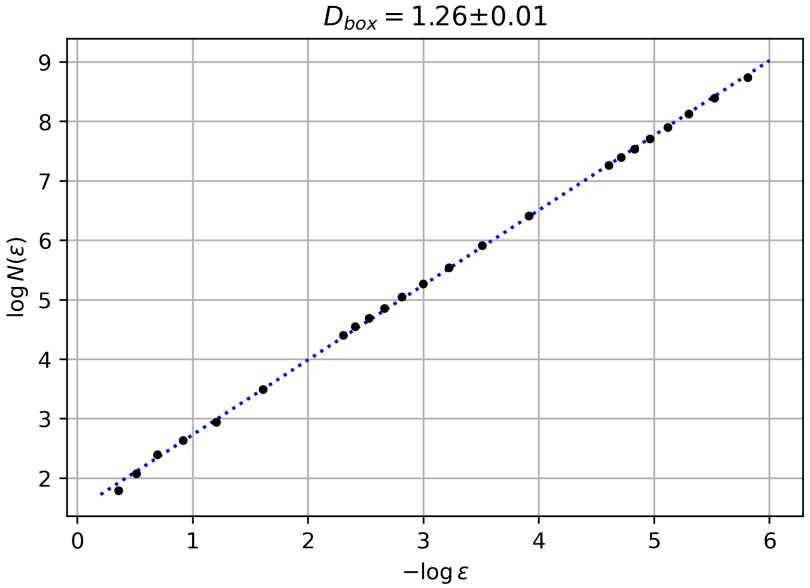

Figure 19: Box-counting dimension for $a = 1.4$ and $b = 0.3$.

Figure 19 presents a plot of $\log N(\epsilon)$ versus $-\log \epsilon$, where the box-counting dimension is computed as the slope of the least-squares linear fit. The estimated value is $D_{box} = 1.26 \pm 0.01$, where this represents the 95% confidence interval for a standard ordinary least-squares linear regression. This value is close the estimate 1.261 ± 0.003 by Russel et al., 1980, although the error is smaller for this estimate.

This does in fact show that the Hénon attractor, for $a = 1.4$ and $b = 0.3$, has non-integer box-counting dimension. This provides further validity to the claim that the Hénon attractor can be considered a fractal in $\mathbb{R}^2$. Since $1 < D_{box} < 2$, this shows that the attractor should be considered as something more than a one-dimensional manifold, which have box-counting dimension 1, in terms of how it occupies space, and that it does not occupy space as if a set with nonzero two-dimensional volume would, which have box-counting dimension 2. This result ties in rather well with the observation of section 3.2 and figure 4, where we observed that the attractor appears to be a product of a one-dimensional manifold with a Cantor set. The fact that the integer part of D_{box} is 1 is due to the one-dimensional manifolds, and the remaining fraction is due to the fact that these one-dimensional manifolds are folded on top each other in a fractal manner similar to a Cantor set.

6.1.2 Lyapunov Dimension

The Lyapunov dimension is based on a conjecture relating the Lyapunov spectrum of an attractor to its capacity dimension. The formula for the Lyapunov dimension was presented in the lecture notes of James Kaplan and James Yorke, where it was conjectured that its value was equal to that of the capacity dimension (Kaplan & Yorke, 1979). For this reason, the dimension is also commonly referred to as the Kaplan-Yorke dimension.

Definition 6.3 (Lyapunov Dimension)**.** *Suppose $\lambda_1 \geq \ldots \geq \lambda_n$ are the Lyapunov exponents of an orbit tending towards an attractor Λ of $F : \mathbb{R}^n \to \mathbb{R}^n$. If $j \geq 0$ is the largest integer such that*

$$\sum_{k=1}^{j} \lambda_k \geq 0,$$

then the Lyapunov dimension is defined as

$$D_L = j + \frac{\sum_{k=1}^{j} \lambda_k}{|\lambda_{j+1}|}. \tag{23}$$

Here it is assumed that the largest integer $j \geq 0$ with $\sum_{k=1}^{j} \lambda_k \geq 0$ also satisfies $j < n$ such that λ_{j+1} exists. By proposition 5.12, this is necessarily the case for attractors of dissipative systems, for which the conjecture was formulated (Grassberger & Procaccia, 1983; Kaplan & Yorke, 1979).

In their lectures notes, Kaplan and Yorke present the numerical observations for a family of two-dimensional and three-dimensional discrete dynamical systems which the conjecture $D_{cap} = D_{KY}$ was based on (Kaplan & Yorke, 1979). However, in Frederickson et al., 1983, of which Kaplan and Yorke are co-authors, they explained that the conjecture should be abandoned since the Lyapunov spectrum can be susceptible to exceptional cases and statistical noise, whereas the capacity dimension is a constant value for a given attractor. Instead of fully dropping the conjecture, they proposed an alternative conjecture that the Lyapunov dimension is equal to the probability dimension, which is an ergodic measure that we shall not cover to avoid a full digression into ergodic theory but refer the interested reader to Grassberger and Procaccia, 1983, Eckmann and Ruelle, 1985 and Parker and Chua, 1989.

In addition, in Frederickson et al., 1983, they present a plausibility argument to give further credibility to this new conjecture. Interestingly, an almost identical argument to the plausibility argument presented by Frederickson et al., 1983, in support of the new conjecture, is used to motivate the plausibility of the old conjecture by Parker and Chua, 1989. The following argument is an adaptation of this plausibility argument in support of the old conjecture, i.e., $D_L = D_{cap}$.

Suppose $\lambda_1 \geq \ldots \geq \lambda_n$ are the Lyapunov exponents of an attractor of $F : \mathbb{R}^n \to \mathbb{R}^n$. Consider an n-dimensional cube $C(0)$, with sufficiently small side length $\epsilon > 0$, centered at some point x for which the orbits tends towards the attractor. Now denote $C(k)$ as the image of F^k of $C(0)$. Also suppose, with a suitable rotation of the cube, that the length of the ith side of $C(n)$ approximately evolves as ϵe^{λ_i} for sufficiently large n. Now, if $1 \leq j < n$ is some arbitrary j such that $\lambda_{j+1} < 0$ and $N(k)$ is the number of cubes of side length $\epsilon e^{\lambda_{j+1} k}$ required to cover $C(k)$, we see that

$$N(k) \approx \prod_{i=1}^{j} \left(\frac{\epsilon e^{\lambda_i k}}{\epsilon e^{\lambda_{j+1} k}} \right) = e^{\left(\sum_{i=1}^{j} \lambda_i - j\lambda_{j+1}\right) k}, \tag{24}$$

since the sides corresponding to $\lambda_i \leq \lambda_{j+1}$, with $j + 1 < i \leq n$, shrink with respect to $e^{\lambda_{j+1} k}$ such that they do not influence $N(k)$ for sufficiently large k.

Using 24, we define $D_{cap}(j)$, and see that,

$$\begin{aligned} D_{cap}(j) &:= \lim_{k\to\infty} -\frac{\log N(k)}{\log(\epsilon e^{\lambda_{j+1}k})} \\ &= \lim_{k\to\infty} -\frac{\left(\sum_{i=1}^{j}\lambda_i - j\lambda_{j+1}\right)k}{\lambda_{j+1}k + \log\epsilon} \\ &= j - \frac{\sum_{i=1}^{j}\lambda_i}{\lambda_{j+1}} \\ &= j + \frac{\sum_{i=1}^{j}\lambda_i}{|\lambda_{j+1}|}. \end{aligned}$$

Then, proceed to define $D_{cap}(j)$ in a similar manner for all $1 \leq j < n$ such that $\sum_{i=1}^{j}\lambda_i \geq 0$. It is shown in Frederickson et al., 1983 that the minimum $D_{cap}(j)$ is attained at the largest integer j such that $\sum_{i=0}^{n}\lambda_j \geq 0$. Using this largest integer j such that $\sum_{i=1}^{j}\lambda_i \geq 0$, with some abuse of notation, this then gives the approximation

$$\begin{aligned} D_{cap} &= \lim_{\epsilon\to 0^+} -\frac{\log N(\epsilon)}{\log\epsilon} \\ &\approx \lim_{k\to\infty} \frac{\log N(k)}{\log(\epsilon e^{\lambda_{j+1}k})} \\ &= j + \frac{\sum_{i=0}^{j}\lambda_i}{|\lambda_{j+1}|} \\ &= D_L, \end{aligned}$$

which concludes the plausibility argument. It should be noted that it is implicitly assumed that the initial hypercube $C(0)$ eventually 'spreads out' over the entire attractor such that, for sufficiently large k, the estimate $N(k)$ also corresponds well with the estimate of the number of boxes of side length $\epsilon e^{\lambda_{j+1}k}$ required to cover the the attractor.

Using formula 23, this allows for a straightforward computation of the Lyapunov dimension of the Hénon attractor. For instance, for $a = 1.4$ and $b = 0.3$, the approximated Lyapunov exponents for an orbit in the basin of attraction of the attractor are $\lambda_1 = 0.421\ldots$ and $\lambda_2 = -1.625\ldots$, which gives $D_L = 1.259\ldots$ for the Lyapunov dimension. This value is quite close to the estimate of the box-counting dimension of figure 19. Despite the fact that the box-counting dimension is not necessarily equal to the capacity dimension, and the fact that the conjecture $D_L = D_{cap}$ should be dropped according to Kaplan and Yorke, they still provide good estimates that are generally quite close to D_{cap} (Eckmann & Ruelle, 1985; Pikovsky & Politi, 2016).

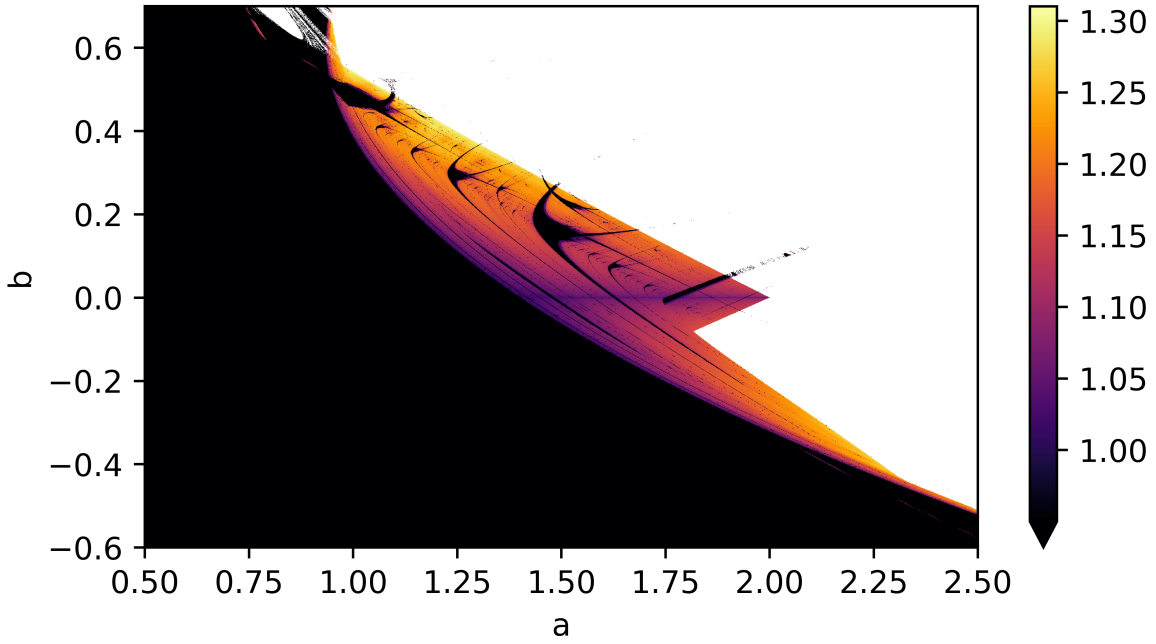

Figure 20: Lyapunov dimension in a 1500×1500 parameter plane with $0.5 < a < 2.5$ and $-0.6 < b < 0.7$. The black regions correspond to a Lyapunov dimension of 0 and the white regions correspond to cases where no attractor was detected.

By using the same data used to generate the Lyapunov diagram of figure 14, we can use formula 23 to compute the Lyapunov dimension in this parameter plane, where figure 20 shows the result. The largest Lyapunov dimension for this parameter grid is $D_L \approx 1.31$ which is attained at the parameter values $a \approx 1.021$ and $b \approx 0.530$.

6.2 Stable and Unstable Manifold

In the preliminary section, in definition 2.7, we defined hyperbolic fixed points of a C^1 map as either attracting, repelling, or a saddle according to the eigenvalue spectrum of the linearization at that fixed point. The classification of the former two can be motivated by the result of theorem 2.5 and corollary 2.6. However, as of yet, no such result was presented for saddle fixed points.

In the cases where x is a saddle fixed point of a diffeomorphism F, it turns out that, in a neighbourhood of x, the points that tend towards x upon iteration of F assume the structure of a smooth manifold, commonly referred to as the local stable manifold. In addition, the global set of points that tend towards x upon iteration of F, also referred to as the stable manifold, can be constructed from this local stable manifold. A similar result can be shown for the set of points that converge to x upon iteration of its inverse F^{-1}, where these sets are called the local unstable manifold and the unstable manifold, respectively.

For purposes of simplicity, we restrict relevant results and the construction of the stable and unstable manifold to saddle fixed points of $F : \mathbb{R}^2 \to \mathbb{R}^2$, where F is a diffeomorphism.

Theorem 6.4 (Local Unstable Manifold Theorem)**.** *Suppose x is a saddle fixed point of a diffeomorphism $F : \mathbb{R}^2 \to \mathbb{R}^2$. Then, there exists $\delta > 0$ and a C^1 curve $\gamma : (-\delta, \delta) \to \mathbb{R}^2$ such that*

1. $\gamma(0) = x$.
2. $\gamma'(0) \neq 0$.
3. $\gamma'(0)$ *is an unstable eigenvector of DF_x, i.e., associated to the eigenvalue with $|\lambda| > 1$.*
4. γ *is F^{-1} invariant, i.e., points in the image of γ are mapped to the image of γ by F^{-1}.*
5. $F^{-n}(\gamma(t)) \to x$ *as $n \to \infty$ for any $t \in (-\delta, \delta)$.*
6. *There exists $\epsilon > 0$ such that if $||F^{-n}(y) - x|| < \epsilon$ for all $n \geq 0$, then $y = \gamma(t)$ for some $t \in (-\delta, \delta)$.*

We shall not provide a detailed proof of this theorem and instead refer the reader to Devaney, 2003.

The curve γ, satisfying the conditions of theorem 6.4, is then referred to as the local unstable manifold at x and is commonly denoted by γ_u. Similarly, since F is a diffeomorphism, the local unstable manifold at x, when considered as a fixed point of the diffeomorphism F^{-1}, is the stable manifold at x of F denoted by γ_s. These local curves then allow for a definition of the stable and unstable manifold.

Definition 6.5 (Stable and Unstable Manifold)**.** *Suppose x is a saddle fixed point of the a diffeomorphism $F : \mathbb{R}^2 \to \mathbb{R}^2$ and γ_s and γ_u are the local stable and local unstable manifold at x. The stable manifold $W^s(x)$ and unstable manifold $W^u(x)$ at x are defined as*

$$W^s(x) = \bigcup_{n=1}^{\infty} F^{-n}(\gamma_s), \quad \textit{and} \quad W^u(x) = \bigcup_{n=1}^{\infty} F^{n}(\gamma_u), \tag{25}$$

where γ_s and γ_u are considered as subsets of $\mathbb{R}^2$, i.e., as their image in $\mathbb{R}^2$ (Devaney, 2003).

From this definition and theorem 6.4 it is then straightforward to show the following result.

Proposition 6.6. *Suppose $W^s(x)$ and $W^u(x)$ are the stable and unstable manifold of a saddle fixed point of the diffeomorphism $F : \mathbb{R}^2 \to \mathbb{R}^2$. Then $W^s(x)$ and $W^u(x)$ satisfy*

$$W^s(x) = \{y \in \mathbb{R}^2 : F^n(y) \to x \text{ as } n \to \infty\}, \quad \text{and} \quad W^u(x) = \{y \in \mathbb{R}^2 : F^{-n}(y) \to x \text{ as } n \to \infty\}.$$

Proof. We will only show the proof for the equality regarding $W^u(x)$, since the equality for $W^s(x)$ is shown in a completely similar manner by observing that it is the unstable manifold of x when considered as a saddle fixed point of the inverse F^{-1}.

Suppose γ_u is the local unstable manifold of x that satisfies the conditions of theorem 6.4. Then, by definition of the unstable manifold 6.5, the unstable manifold satisfies

$$W^u(s) = \bigcup_{n=1}^{\infty} F^{-n}(\gamma_u).$$

Using this equality, we observe that proving the proposition is equivalent to showing that $F^{-n}(y) \to x$ as $n \to \infty$ if and only if $F^{-m}(y) \in \gamma_u$ for some $m > 0$, where γ_u is considered as a subset of $\mathbb{R}^2$. To this end, suppose $F^{-n}(y) \to x$ as $n \to \infty$ for some $y \in \mathbb{R}^2$. Then, by the 6th condition of theorem 6.4, there exists $\epsilon > 0$ such that if $||F^{-n}(z) - x|| < \epsilon$ for all $n \geq 0$, then necessarily $z \in \gamma_u$. Now, since $F^{-n}(y) \to x$ as $n \to \infty$, there exists some $m > 0$ such that $||F^{-n}(y) - x|| < \epsilon$ for all $n \geq m$. This then gives that $||F^{-n}\left(F^{-m}(y)\right) - x|| < \epsilon$ for all $n \geq 0$, which implies that $F^{-m}(y) \in \gamma_s$ and shows the first direction. The reverse direction is trivial to show as it is a direct implication of the 5th condition of theorem 6.4. This concludes the proof. □

Despite the fact that theorem 6.4 is only an existence proof, the 5th condition, namely that $\gamma'(0)$ is tangent to the unstable eigenvector of DF_x, borrowing the notation of the theorem, still allows for a relatively straightforward method to numerically estimate segments of the unstable manifold. Namely, suppose we pick some large collection of initial points along both directions of the unstable eigenvector in sufficiently close proximity to the saddle point. Then, these points should lie on or in very close proximity to the local unstable manifold. Hence, by definition 6.5, connecting this collection of initial points and their images for a few iterations by line segments should give an approximation to a segment of the unstable manifold. In a similar manner we can give an approximation to a segment of the stable manifold by numerically computing it as the unstable manifold of the inverse. An informed implementation of this method requires a few more technicalities that are included in the appendix A.3.

Figure 21 provides a numerical estimate of a segment of both the stable and unstable manifold of the saddle fixed point (x_+, y_+) (see 5) for $a = 1.4$ and $b = 0.3$. We again stress that this is only a segment of the stable and unstable manifold. Also, of the segment of the stable manifold computed, the figure only shows the part of it that lies in the region of the plane depicted in figure 21. The stable manifold was significantly harder to compute since the segment corresponding to the upward direction of the stable eigenvector seemed to diverge towards infinity relatively quickly. The unstable manifold does not present such difficulties as the saddle fixed point (x_+, y_+) and points in close proximity to it along the direction of the unstable eigenvector are contained in the trapping region described in section 3 and shown in figure 5. This causes the unstable manifold to be completely contained in this trapping region.

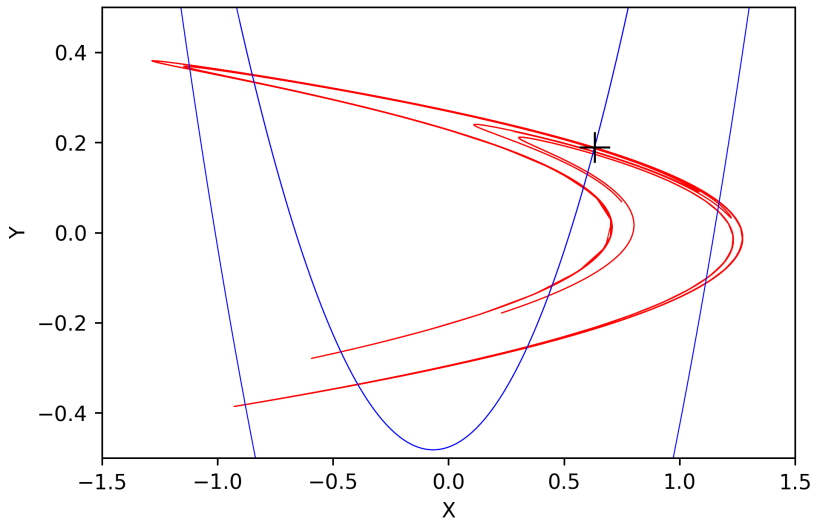

Figure 21: Segment of the stable manifold (blue) and the unstable manifold (red) of the saddle fixed point (x_+, y_+) (black marker) for $a = 1.4$ and $b = 0.3$ in some region of the plane.

What is even more remarkably is that visually the unstable manifold appears to closely resemble the shape of the attractor depicted in figure 4. This relation between the unstable manifold and the attractor of the Hénon map is, in fact, the topic of the main theorem presented by Benedicks and Carleson, 1991, which is proven by means of rigorous analysis.

Theorem 6.7 (Main result of Benedicks and Carleson, 1991)**.** *Suppose W^u is the unstable manifold of the fixed point (x_+, y_+) of $H_{a,b}$. Then for all $c < \log 2$ there is a $b_0 > 0$ such that for all $b \in (0, b_0)$ there is a set $E(b)$ with positive one-dimensional Lebesgue measure such that for all $a \in E(b)$:*

1. *There is an open set $U_{a,b}$ such that for all $(x, y) \in U_{a,b}$,*

$$d(H^n_{a,b}(x, y), \overline{W^u}) \to 0 \text{ as } n \to \infty.$$

2. *There exists a $(x_0, y_0) \in \overline{W^u}$, which depends on both a and b, such that*
   (a) *the forward orbit of (x_0, y_0) is dense in W^u;*
   (b) *$||(DH^n_{a,b})_{(x_0,y_0)}(0, 1)|| \geq e^{nc}$ for all $n \geq 0$.*

Here $d(x, A) := \inf_{y \in A} ||x - y||$ for $x \in \mathbb{R}^2$ and $A \subset \mathbb{R}^2$.

This theorem does in fact prove that, for such parameter values and a particular $c < \log 2$, there exists an attractor that is equal to the closure of the unstable manifold of the fixed point (x_+, y_+), where the attractor is an attractor in terms of definition 5.10. To see why, suppose $b \in (0, b_0)$ and $a \in E(b)$, then the existence of a point $(x_0, y_0) \in \overline{W^u}$ whose forward-orbit is dense in $\overline{W^u}$ also implies that its ω-limit set is equal to $\overline{W^u}$, that is $\omega((x_0, y_0)) = \overline{W^u}$. In addition, because there exists a set of positive two-dimensional Lebesgue measure, namely the open set $U_{a,b}$, such that $\omega((x, y)) \subset \overline{W^u} = \omega((x_0, y_0))$ for all $(x, y) \in U_{a,b}$, it follows by definition 5.10 that $\Lambda := \omega((x_0, y_0))$ is an attractor with $\Lambda = \overline{W^u}$.

The theorem also shows that, for values of $0 < c < \log 2$, this is a chaotic attractor in terms of definition 5.9. Namely, for $b \in (0, b_0)$ and $a \in E(b)$, the existence of an orbit $(x_0, y_0) \in \Lambda$ such that $||(DH^n)_{a,b}(0, 1)||_{(x_0,y_0)} \geq e^{cn}$ for all $n \geq 0$ shows that the largest Lyapunov exponent λ_1 of this

orbit is strictly positive. In addition, since $\lambda_1 + \lambda_2 = \log(|b|)$, by corollary 5.13, this also implies that $\lambda_2 = \log(|b|) - \lambda_1 < 0$ because $0 < b < b_0 < 1$. Then, because the forward orbit of (x_0, y_0) is dense in W^u, where W^u clearly does not correspond to a periodic cycle, it follows that (x_0, y_0) is not asymptotically periodic. So, since the orbit of (x_0, y_0) is not asymptotically periodic and $\lambda_1 > 0$ and $\lambda_2 < 0$, it follows that the orbit of $(x_0, y_0) \in \Lambda$ is chaotic in terms of definition 5.8, which implies by definition 5.9 that Λ is a chaotic attractor. For convenience, we summarize this in the following corollary.

Corollary 6.8. *There exists a $b_0 > 0$ such that for any $b \in (0, b_0)$ there exists a set $E(b)$, with positive one-dimensional Lebesgue measure, such that, for all $a \in E(b)$, $H_{a,b}$ has a chaotic attractor Λ in terms of definition 5.9 with $\Lambda = \overline{W^u}$, where W^u is the unstable manifold of the saddle fixed point (x_+, y_+).*

It should be noted that theorem 6.7 is an existence proof and that the theorem does not specify any particular value of b_0. As a result, it is not clear whether the parameter values of $a = 1.4$ and $b = 0.3$ are included. Although, it is mentioned in Broer and Takens, 2009 that the value $b = 0.3$ is probably far too large to be included with the approach taken by Benedicks and Carleson, 1991.

Despite the fact that it is doubtful whether the values $a = 1.4$ and $b = 0.3$ are included in the parameter set of the theorem, it still becomes evident from numerical observations such as figure 21 and figure 4 that an equality of the attractor and the closure of the unstable manifold seems plausible. Due to such observations and the work of Benedicks and Carleson, 1991, chaotic attractors that are equal to the closure of an unstable manifold of a saddle periodic point, or a saddle equilibrium point in continuous dynamical systems, are also referred to as Hénon-like attractors (Broer & Takens, 2009).

From figure 21, we also see that the stable and unstable manifold seem to intersect at points different from (x_+, y_+). In addition, they seem to do so in a manner such that the stable and unstable manifold are not tangent at these intersections. Such points are also called transversal homoclinic intersections and where used to give a proof of a chaotic set of the Hénon map before the result of Benedicks and Carleson, 1991. Namely, as shown by Smale, 1967, the existence of a homoclinic intersection can be used to construct a Horseshoe map which is topologically conjugate to the shift automorphism on two symbols. Then, since the shift automorphism is chaotic in the sense of definition 2.14, this proves the existence of a set where the dynamics of the Hénon map are chaotic (Devaney, 2003).

However, although it proves the existence of a chaotic set, the proof does not specify whether this set is also an attractor (Devaney & Nitecki, 1979; Marotto, 1979). Hence, this result is weaker than the main theorem 6.7 of Benedicks and Carleson, 1991. For this reason, we do not cover the result in detail. For an extensive discussion on the Horseshoe map and the shift automorphism, we refer the reader to Devaney, 2003. For an existence proof of homoclinic intersections in the Hénon map, for some parameter values, we refer the reader to Marotto, 1979. For a direct construction of a Horsehoemap and a topological conjugacy with the shift automorphism, for a map that the Hénon map is conjugate to, we refer the reader to Devaney and Nitecki, 1979.

7 Concluding Remarks

As a final note, we briefly summarize what was covered. We conclude with a few recommendations for further reading.

In section 3, we gave a brief overview of Lorenz' article *Deterministic Nonperiodic Flow* and the Lorenz system (Lorenz, 1963). Then, we showed Hénon's construction of the two-dimenional quadratic map, which was later named the Hénon map, along with its similarities to the Lorenz system and its attractor.

In section 4, we classified the stability of fixed points of the Hénon map. We also identified two curves, in the parameter plane, where period doubling bifurcation occur. We then presented numerical evidence of a period doubling cascade and identified the possibility that there are chaotic regions in the parameter plane.

In order to further analyse the regions where the dynamics appear chaotic, we relied on the concept of Lyapunov exponents. We presented and gave plausibility arguments for heuristics, for numerical purposes, to classify the system's behavior and its attractor by means of Lyapunov exponents. Accordingly, we then classified the stability and attractor type of the Hénon map by means of a Lyapunov diagram. In this Lyapunov diagram, we observed numerical evidence of a set, which appears to have positive two-dimensional Lebesgue measure, where the dynamics and the attractor of the Hénon map can be classified as chaotic.

Lastly, in section 6, we discussed some properties of the attractor of the Hénon map. Firstly, we gave numerical estimates of some fractal dimensions, namely the box-counting dimension and the Lyapunov dimension, where we also presented a motivating discussion for these dimensions along with their relation to each other. Lastly, we presented a numerical estimate of a segment of the stable and unstable manifold of one of the Hénon map's saddle fixed points. We also discussed the relation that the unstable manifold and the attractor of the Hénon map appear to have and related this to the work of Benedicks and Carleson, 1991.

For further reading regarding dynamical systems and chaos, we suggest Broer and Takens, 2009 and Devaney, 2003. For an accessible book that explains numerical methods for dynamical systems, we recommend Parker and Chua, 1989. Lastly, for an accessible book on Lyapunov exponents and their uses, the textbook Pikovsky and Politi, 2016 is a good start. For a more formal and rigorous discussion of Lyapunov exponents, we refer the reader to Viana, 2014.

A Numerical Methods and Considerations

A.1 Lyapunov Exponents

For the computation of the Lyapunov spectrum, the method developed by Benettin et al., 1980 was used. In Parker and Chua, 1989, this method is motivated by means of an intuitive explanation. Below, we present an adaptation of this explanation. The notation for the algorithm is similar to that of Garst, 2018.

First, suppose $F : \mathbb{R}^2 \to \mathbb{R}^2$ is C^1 and $x \in \mathbb{R}^2$ with Lyapunov exponents $\lambda_1 \geq \lambda_2$. Then, by theorem 5.2, it follows that

$$\lambda_1 = \lim_{n\to\infty} \frac{1}{n} \log ||(DF^n)_x v||$$

for almost all $v \in \mathbb{R}^2$, except for possibly a subspace with Lebesgue measure zero. Hence, for some random $v \in \mathbb{R}^2$, with uniformly chosen direction, the Lyapunov exponent at x in the direction of v is the largest Lyapunov exponent λ_1 with probability 1.

Computing λ_1:
Relying on this observation, it is relatively straightforward to compute the largest Lyapunov exponent. Namely, pick some arbitrary $v \in \mathbb{R}^2$ with unit length and choose some integer $s \geq 1$ that specifies after how many iterations we apply a normalization. Then, set $v_0 = v$ and $x_0 = x$ and iterate the following scheme

$$\begin{aligned} u_{k+1} &= (DF^s)_{x_{ks}} v_k, \\ v_{k+1} &= \frac{u_{k+1}}{||u_{k+1}||}, \\ x_{(k+1)s} &= F^s(x_{ks}), \end{aligned}$$

for $0 \leq k \leq N-1$, where we write x_{ks} instead of x_k to make it explicit that it is the ks-th point along the orbit of x_0.

Then, it follows that

$$\begin{aligned} & u_{k+1} = (DF^s)_{x_{ks}} v_k \\ \implies & ||u_k|| u_{k+1} = (DF^s)_{x_{ks}} u_k \\ \implies & ||u_k|| u_{k+1} = (DF^s)_{x_{ks}} \circ (DF^s)_{x_{(k-1)s}} v_{k-1} \\ \implies & ||u_k|| u_{k+1} = (DF^{2s})_{x_{(k-1)s}} v_{k-1}, \end{aligned}$$

for $1 \leq k \leq N-1$, where we implicitly used the chain rule. Using this, it is straightforward to show, by means of induction, that

$$\prod_{k=1}^{N} ||u_k|| = ||(DF^{Ns})_{x_0} v_0||.$$

Then, since the Lyapunov exponent at x_0 in the direction of v_0 is λ_1 with probability 1 and, assuming this is the case,

$$\begin{aligned}\lambda_1 &= \lim_{n\to\infty} \frac{1}{n} \log ||(DF^n)_{x_0} v_0|| \\ &\approx \frac{1}{sN} \log ||(DF^{sN})_{x_0} v_0|| \\ &= \frac{1}{sN} \log \left(\prod_{k=1}^{N} ||u_k|| \right) \\ &= \frac{1}{sN} \sum_{k=1}^{N} \log ||u_k||,\end{aligned}$$

for sufficiently large N.

Computing λ_1 and λ_2:
Although the method of picking some random v_0, with uniformly chosen direction, is quite useful for computing λ_1, it is not well-suited for the computation of the full Lyapunov spectrum at x_0, since the probability of observing λ_2 for such a direction is 0.

To derive a more suitable method, we rely on proposition 5.12 and a useful approximation. Namely, using the ellipse analogy of section 5.1, we see that a small circle $E(0)$ around x_0 evolves as an ellipse $E(n)$ centered at F^n when approximating F^n by its linearization $(DF^n)_{x_0}$. In addition, by the result of theorem 5.2, the expansion/contraction along the major axis of the ellipse is proportional to $e^{\lambda_1 n}$ and the expansions/contraction along the minor axis, which is orthogonal to the major axis, is proportional to $e^{\lambda_2 n}$. This implies that when $|E(n)|$ is the 2-dimensional volume of the ellipse as a function of n that then, for sufficiently large n,

$$|E(n)| \approx Ce^{(\lambda_1+\lambda_2)n},$$

for some constant $C > 0$, which gives

$$\lambda_1 + \lambda_2 \approx \lim_{n\to\infty} \frac{1}{n} \log |E(n)|. \tag{26}$$

Using this relation, we can derive an algorithm that computes both λ_1 and λ_2. Namely, choose some $v_{0,1}$ with unit length and $v_{0,2}$, with unit length, orthogonal to $v_{0,1}$. Then, the square $C(0)$ at x_0 with sides $v_{0,1}$ and $v_{0,2}$ has 2-dimensional volume $|C(0)| = ||v_{0,1}|| \cdot ||v_{0,2}|| = 1$. Now, pick some $s \geq 1$, not too large, and iterate the following scheme for $0 \leq k \leq N-1$:

$$\begin{aligned}\tilde{u}_{k+1,1} &= (DF^s)_{x_{ks}} v_{k,1}, \\ \tilde{u}_{k+1,2} &= (DF^s)_{x_{ks}} v_{k,2}, \\ u_{k+1,1} &= \tilde{u}_{k+1,1}, \\ u_{k+1,2} &= \tilde{u}_{k+1,2} - (\langle \tilde{u}_{k+1,2}, u_{k+1,1} \rangle / \langle u_{k+1,1}, u_{k+1,1} \rangle)\, u_{k+1,1}, \\ v_{k+1,1} &= \frac{u_{k+1,1}}{||u_{k+1,1}||}, \\ v_{k+1,2} &= \frac{u_{k+1,1}}{||u_{k+1,1}||}, \\ x_{(k+1)s} &= F^s(x_{ks}).\end{aligned}$$

Denote $C(n)$ by the image of the square $C(0)$ of $(DF^n)_{x_0}$ and denote its 2-dimensional volume by $|C(n)|$. Then, we see that

$$|C(sN)| = \prod_{k=1}^{N} \frac{|C(sk)|}{|C(s(k-1)|}, \tag{27}$$

since $|C(0)| = 1$. From the construction of the algorithm, we have

$$\frac{|C(s)|}{|C(0)|} = ||u_{1,1}|| \cdot ||u_{1,2}||,$$

because the 2-dimensional volume of the parallelogram $C(s)$ with sides $\tilde{u}_{1,1}$ and $\tilde{u}_{1,1}$ is equal to the 2-dimensional volume of the cube with sides $u_{1,1}$ and $u_{1,2}$.

Then, as opposed to calculating the exact value of $|C(sk)|/|C(s(k-1))|$ for $k > 1$, the algorithm calculates the average contraction/stretching along these s iterations by means of constructing a new square with sides of length 1, with the Gram-Schmidt orthonormalization procedure, and then applying a similar procedure to how $|C(s)|/|C(0)|$ was computed. This gives the useful approximation

$$\frac{|C(sk)|}{|C(s(k-1))|} \approx \frac{||u_{k,1}|| \cdot ||u_{k,2}||}{||v_{k-1,1}|| \cdot ||v_{k-1,2}||} = ||u_{k,1}|| \cdot ||u_{k,2}||.$$

Now, substituting this into 27 gives

$$|C(sN)| \approx \prod_{k=1}^{N} ||u_{k,1}|| \cdot ||u_{k,2}||,$$

which, combined with 26, shows that

$$\begin{aligned} \lambda_1 + \lambda_2 &\approx \lim_{n\to\infty} \frac{1}{n} \log |C(n)| \\ &\approx \frac{1}{sN} \log |C(sN)| \\ &\approx \frac{1}{sN} \log \left(\prod_{k=1}^{N} ||u_{k,1}|| \cdot ||u_{k,2}|| \right) \\ &= \frac{1}{sN} \sum_{k=1}^{N} \log ||u_{k,1}|| + \frac{1}{sN} \sum_{k=1}^{N} \log ||u_{k,2}||, \end{aligned} \tag{28}$$

provided $N \geq 1$ is sufficiently large.

Now, when we observe the iteration scheme, we see that the values associated to $u_{k,1}$ are actually the exact same values as the u_k values that the algorithm that computes λ_1 would generate. This gives the useful relation

$$\lambda_1 \approx \frac{1}{sN} \sum_{k=1}^{N} \log ||u_{k,1}||,$$

which, upon substitution into the result of 28, gives

$$\lambda_2 \approx \frac{1}{sN} \sum_{k=1}^{N} \log ||u_{k,2}||.$$

Hence, this gives the approximation of the Lyapunov exponents as

$$\begin{aligned} \lambda_1 &\approx \frac{1}{sN} \sum_{k=1}^{N} \log ||u_{k,1}||, \\ \lambda_2 &\approx \frac{1}{sN} \sum_{k=1}^{N} \log ||u_{k,2}||. \end{aligned} \tag{29}$$

This method can also be generalized to compute the Lyapunov spectrum for higher dimensional cases by a similar algorithm that relies on the Gram-Schmidt orthonormalization procedure.

From the construction of the algorithm, we also see that the linearization along the orbit always has to be nonsingular, since otherwise the Gram-Schmidt orthonormalization procedure fails.

Numerical considerations and implementation:
For the implementation of the algorithm that computes the full Lyapunov spectrum, we specifically tailored it to be used for the Hénon map, where a general implementation could also have been used but was not necessary. The code is given below.

```
import numpy as np

Henon = lambda x, a, b : [x[1] + 1 - a*(x[0]**2), b*x[0]]
JacobianHenon = lambda x, a, b : [[-2*a*x[0], 1], [b, 0]]

def HenonOrbit(x0, a, b, iterations = int(1e4)):
    X = np.zeros([2, iterations])
    X[:,0] = x0
    for i in range(1,iterations):
        X[:, i] = Henon(X[:,i-1], a, b)
        if np.linalg.norm(X[:, i]) > 1e3:
            X = np.array([ X[0][0:i+1] , X[1][0:i+1] ])
            return X, False
    return X, True

def Lyapunov(a, b, N_t = int(1e3), N = int(1e4), x0 = [0, 0]):

    Xlist, condition = HenonOrbit(x0, a, b, iterations= N_t + N )

    if condition == False:
        bounded = False
        lyapunov1, lyapunov2 = None, None
    else:
        bounded = True
        U = np.identity(2)
        Unorm = np.zeros((2,N))

        for i in range(N):

            X = Xlist[:,N_t+i]
            DHx = JacobianHenon(X, a, b)
            V = np.matmul(DHx, U)
            U[:,0] = V[:,0]
            U[:,1] = V[:,1] - ( np.dot(V[:,1], U[:,0]) / np.dot(U[:,0],U[:,0]) ) * U[:,0]
            Unorm[0,i] = np.linalg.norm(U[:,0])
            Unorm[1,i] = np.linalg.norm(U[:,1])
            U[:,0] /= Unorm[0,i]
            U[:,1] /= Unorm[1,i]
```

```
            lyapunov1 = (1/N) * np.sum(np.log(Unorm[0,::]))
            lyapunov2 = (1/N) * np.sum(np.log(Unorm[1,::]))
            if math.isnan(lyapunov1) == True or math.isnan(lyapunov2) == True:
                lyapunov1, lyapunov2, bounded = None, None, False

    return lyapunov1, lyapunov2, bounded
```

Notice that the algorithm will only compute the Lyapunov exponents of orbits that stay bounded in some region. This was done since we are primarily interested in orbits that stay bounded and tend towards some attractor. Also, since the Lyapunov spectrum is generally the same for all points in the basin of attraction of a particular attractor (see remark 5.4), the transient behaviour of the orbit is irrelevant for the limiting value that defines the Lyapunov exponent. For this reason, we only calculate the Lyapunov exponents from the last N iterations of an orbit of $N_t + N$ iterations, where the subscript t is used to denote transient.

Furthermore, the algorithm we used performs the Gram-Schmidt orthonormalization procedure after each iteration, as opposed to after each $s > 1$ subsequent iterations. The reason for this is that the method is generally more stable when applying this procedure after each iteration, despite requiring more operations and taking up more time. For instance, initially the algorithm was implemented allowing for a a general $s \geq 1$. However, after testing this method by using it to generate Lyapunov diagrams, it was observed that the method was not as accurate for parameter values with b close to zero when $s > 1$. This is likely due to the fact that $|\det(DH_{a,b})| = |b|$, i.e., the determinant is also close to 0 for such parameter values. This causes volumes to contract quite rapidly which makes the approximation of the Lyapunov exponents less accurate provided the Gram-Schmidt procedure is not used after each iteration.

This algorithm was used to generate the data for all figures of section 5.3 and section 6.1.2. In addition, for all of these figures the values $N_t = 10^3$ and $N = 10^4$ were used similar to what was done by Garst, 2018. As opposed to the predefined $x_0 = (0, 0)$, which the algorithm defaults to if no initial point is provided, the initial point was usually taken in close proximity to, but not equal to, (x_+, y_+) (see 5). The parameter grid of the Lyapunov diagrams where chosen with equidistant points such that no parameter value had $b = 0$, since the method only works when the linearization is nonsingular. It took around 50 hours to generate the data for figure 14, figure 16, and figure 20, and the date for figure 17 and figure 18 took around 24 hours each.

A.2 Box-Counting Dimension

In order to compute the box-counting dimension, the box-counting technique was used. In particular, an adaptation of the technique presented in Parker and Chua, 1989. It should be noted that this method only works for sets having finitely many element. Below, a brief explanation of the method is given for finite subsets of $\mathbb{R}^2$, where it can also be generalized to higher dimension with some minor changes.

Compute $N(\epsilon)$:
Suppose, we have a set $M \subset \mathbb{R}^2$, with finitely many elements, and suppose $\epsilon > 0$. Then define, the respective maximum and minimum x-coordinate and y-coordinate by

$$x_{min} := \min_{(x,y)\in A} x, \qquad x_{max} := \max_{(x,y)\in A} x,$$
$$y_{min} := \min_{(x,y)\in A} y, \qquad x_{max} := \max_{(x,y)\in A} y.$$

Also define the integers

$$N_x := \left\lceil \frac{x_{max} - x_{min}}{\epsilon} \right\rceil, \quad N_y := \left\lceil \frac{y_{max} - y_{min}}{\epsilon} \right\rceil,$$

where $\lceil \cdot \rceil$ is the ceiling function that rounds up real numbers to integers. Then, define the matrix A as the zero N_y by N_x matrix. In this way, we can use the matrix A as a representation of a grid of boxes with side length ϵ placed over the set M. In order to count how many of these boxes contain an element of M, we loop over the elements of M and sort them to a box.

Namely, for every $(x, y) \in M$, we can assign integers

$$n_x := \left\lceil \frac{x - x_{min}}{\epsilon} \right\rceil, \qquad n_y := \left\lceil \frac{y - y_{min}}{\epsilon} \right\rceil,$$

where for the cases with $x = x_{min}$, we assign $n_x = 1$, and for the cases with $y = y_{min}$, we assign $n_y = 1$. Because, every $(x, y) \in M$ satisfies $x_{min} \leq x \leq x_{max}$ and $y_{min} \leq y \leq y_{max}$, this implies that $1 \leq n_x \leq N_x$ and $1 \leq n_y \leq N_y$. In this way, we loop over all elements $(x, y) \in M$, where M is a finite set, assign the integers n_x and n_y, and set the entry $a_{n_y n_x}$ to 1, if it is not equal to 1 yet, where a_{ij} is the ijth entry of A.

After this procedure, every element of M is assigned a box in the form of an entry in A marked with a 1 instead of a 0. In addition, an entry of A is only marked with a 1 if it can associated to an element of M and marked with a 0 otherwise. Hence, the number of nonzero elements of A, all marked with a 1, equals the number of boxes of side length ϵ required to cover M for this particular covering. We count, the nonzero entries of A by

$$N(\epsilon) = \sum_{i=1}^{N_y} \sum_{j=1}^{N_x} a_{ij}.$$

Then, this $N(\epsilon)$ is an estimate of the minimum number of boxes of side length ϵ required to cover M. It is only an estimate since this cover might not be optimal cover. Although, for sufficiently small $\epsilon > 0$, it is expected that the estimate is sufficiently close (Parker & Chua, 1989).

Compute D_{box}:
Suppose, we have the same finite set $A \subset \mathbb{R}^2$ as above. In section 6.1.1, we showed that D_{box} approximately satisfies the linear relation

$$\log N(\epsilon) = -D_{box} \log \epsilon + \log k, \tag{30}$$

where $N(\epsilon)$ is the minimum number of boxes of side length $\epsilon > 0$ required to cover A, and k is some real positive constant. Then, we use the method above to estimate $N(\epsilon_i)$ for a collection $\epsilon_i > 0$, sufficiently small but not too small, where $1 \leq i \leq n$. Then, assuming the results have been plotted in a log-log plot to see that the ϵ_i's are chosen such that the relation 30 is approximately linear, we calculate D_{box} as the slope of a standard ordinary-least-squares linear for $\log N(\epsilon_i)$ and $-\log \epsilon_i$ with the error estimate as the standard 95% confidence interval for the slope.

Numerical considerations and implementation:
The method to compute D_{box} was implemented exclusively for the purposes of the Hénon attractor. The code that estimates $N(\epsilon)$ for the Hénon attractor with N points is given below. Note that in order to assign elements to boxes, this method uses the floor function instead of the ceiling function since indices in Python start at 0.

```
import numpy as np
import matplotlib.pyplot as plt


fixpoint1 = lambda a, b : np.array([((b-1)+( (b-1)**2+4*a )**(1/2)) / (2 * a),
                                    b*(((b-1)+( (b-1)**2+4*a )**(1/2)) / (2 * a))])
Henon = lambda x, a, b : [x[1] + 1 - a*(x[0]**2), b*x[0]]


def HenonOrbit(x0, a, b, N = int(1e4)):
    X = np.zeros([2, N])
    X[:,0] = x0
    for i in range(1,N):
        X[:, i] = Henon(X[:,i-1], a, b)
        if np.linalg.norm(X[:, i]) > 1e5:
            X = np.array([ X[0][0:i+1] , X[1][0:i+1] ])
            return X, False
    return X, True

def Boxes(epsilon, a, b, N = int(2e7), N_t = int(1e5)):
    x0 =fixpoint1(a,b) + 0.01*np.array([-1,1])
    X_ = HenonOrbit(x0, a, b, N = N+N_t)

    if X_[1] == True:
        XArray = X_[0]
        X = XArray[0][N_t::]
        Y = XArray[1][N_t::]
        xmax, xmin = np.max(X), np.min(X)
        ymax, ymin = np.max(Y), np.min(Y)
        xboxes = int(np.ceil((xmax-xmin)/epsilon ))
        yboxes =int( np.ceil((ymax-ymin)/epsilon ))
        count = np.zeros((xboxes, yboxes))

        for i in range(len(X)):
            x = X[i]
            y = Y[i]
            xindex = int(np.floor((x-xmin)/epsilon))
            yindex = int(np.floor((y-ymin)/epsilon))
            count[xindex, yindex] = 1
        return np.sum(count)
```

For the computation of the estimate shown in figure 19, the last $2 \cdot 10^7$ iterations of an orbit of $2 \cdot 10^7 + 10^5$ iterations was used to give an estimate of the attractor. The ϵ-values used range from 0.5 to 10^{-4}.

A.3 Unstable Manifold

We only give the method that numerically estimates the unstable manifold of a saddle fixed point $x \in \mathbb{R}^2$ of a diffeomorphism $F : \mathbb{R}^2 \to \mathbb{R}^2$, since the stable manifold is computed as the unstable manifold of the saddle fixed point x of the inverse F^{-1}. The method used to estimate segments of the unstable manifold was found in Garst, 2018, where it is mentioned that the method was based on techniques presented in Broer and Takens, 2009 and Simó, 1992.

As mentioned in section 6.2, the method relies on taking a collection of initial points in close proximity to the saddle fixed point along both directions of the unstable eigenvector of the linearization at the saddle fixed point. Namely, suppose $F : \mathbb{R}^2 \to \mathbb{R}^2$ is a diffeomorphism and x is a saddle fixed point of F. Suppose λ is the unstable eigenvalue of F, i.e., the eigenvalue with an absolute value greater than 1. Also, suppose that $\lambda > 1$ with v a corresponding eigenvector with unit length. Let $\epsilon > 0$, sufficiently small, and suppose we approximate N points on both sides of the local unstable manifold by

$$\begin{aligned} s_j &= \epsilon e^{j \log(\lambda^2)/N}, \\ \omega^L_{0,j} &= x - s_j v, \\ \omega^R_{0,j} &= x + s_j v, \end{aligned}$$

with $j = 1, \ldots, N$, where L and R stand for left and right. By the fifth condition of theorem 6.4, we can indeed expect that these points should provide a sufficiently close approximation to the local unstable manifold, provided ϵ is sufficiently small. The initial points also account for the magnitude of the eigenvalue λ and the fact that it is not desirable for these initial points to be equidistant to each other. The reason for the latter is that too many points near x relative to the points farther removed from x gives a poorer estimate of the unstable manifold, since the line segments connecting the initially farther removed points grow quicker than the line segments corresponding to points initially close (Simó, 1992).

We then iterate the following scheme:

$$\begin{aligned} \omega^L_{k,j} &= F(\omega^L_{k-1,j}), \\ \omega^R_{k,j} &= F(\omega^R_{k-1,j}) \end{aligned}$$

for $1 \leq j \leq N$ and $1 \leq k \leq m$, for some $m \geq 1$ not too large. The estimate of the "left" part of the unstable manifold is then given by connecting the points

$$\omega^L_{0,1}, \ldots, \omega^L_{0,N}, \ldots\ldots, \omega^L_{m,1}, \ldots, \omega^L_{m,N},$$

by line segment, and the estimate of the "right" part of the unstable manifold is given by connecting the points

$$\omega^L_{0,1}, \ldots, \omega^L_{0,N}, \ldots\ldots, \omega^L_{m,1}, \ldots, \omega^L_{m,N},$$

by line segment. Here "right" and "left" are marked with quotation marks since they do not necessarily corresponds to those directions. The name right and left is just a way to distinguish between the two sides of the unstable manifold.

Whenever the dominant eigenvalue λ of DF_x satisfies $\lambda < -1$, the same method can be used by noting that then λ^2 is the dominant eigenvalue of $(DF^2)_x$ with the same eigenvector. In addition, it should be clear by theorem 6.4 and definition 6.5 that the unstable manifold of x when considered as a saddle fixed point of F or when considered as a saddle fixed point of F^2 are the same.

Numerical considerations:
The values for the computation of the unstable manifold of the saddle fixed point (x_+, y_+) where $\epsilon = 10^{-5}$, $N = 10^3$, and $m = 12$. For the computation of the stable manifold, we used the same values for ϵ and N but only computed $m = 7$ iterations, since the error appears to grow quite quickly for more iterations. The code used to generate figure 21 is given below.

```
import numpy as np
import matplotlib.pyplot as plt


fixpoint1 = lambda a, b : np.array([((b-1)+( (b-1)**2+4*a )**(1/2)) / (2 * a),
                                    b*(((b-1)+( (b-1)**2+4*a )**(1/2)) / (2 * a))])
fixpoint2 = lambda a, b : np.array([((b-1)-( (b-1)**2+4*a )**(1/2)) / (2 * a),
                                    b*(((b-1)+( (b-1)**2+4*a )**(1/2)) / (2 * a))])
Henon = lambda x, a, b : [x[1] + 1 - a*(x[0]**2), b*x[0]]
HenonInverse = lambda x, a, b: [x[1]/b, x[0]-1+a*(x[1]**2)/(b**2)]
JacobianHenon = lambda x, a, b : [[-2*a*x[0], 1], [b, 0]]


a, b = 1.4, 0.3
p = fixpoint1(a, b)
DF = JacobianHenon(p, a, b)
eig = np.linalg.eig(DF)
lambda1 = eig[0][0]
lambda2 = eig[0][1]
v1 = eig[1][:, 0]
v2 = eig[1][:, 1]


N = int(1000)
epsilon = 1e-5
mu = 12
ms = 7
Narray = np.arange(1, N+1, step = 1)

WLU = np.zeros((mu, N, 2))
WRU = np.zeros((mu, N, 2))

WLS = np.zeros((ms, N, 2))
WRS = np.zeros((ms, N, 2))


SU = epsilon*np.exp(Narray*np.log(lambda1**4)/N)
SS = epsilon*np.exp(Narray*np.log((1/lambda2)**2)/N)


for i in range(N):

    WLU[0][i] = p-SU[i]*v1
    WRU[0][i] = p+SU[i]*v1

    WLS[0][i] = p-SS[i]*v2
    WRS[0][i] = p+SS[i]*v2

for i in range(1, mu):
    for j in range(N):
        WLU[i][j] = Henon(Henon(WLU[i-1][j], a, b), a, b)
        WRU[i][j] = Henon(Henon(WRU[i-1][j], a, b), a, b)

for i in range(1, ms):
    for j in range(N):
```

```
            WLS[i][j] = HenonInverse(WLS[i-1][j], a, b)
            WRS[i][j] = HenonInverse(WRS[i-1][j], a, b)

for i in range(mu):
    plt.plot(WLU[i,:, 0], WLU[i, :, 1], 'r', linewidth = 1/2)
    plt.plot(WRU[i,:, 0], WRU[i, :, 1], 'r', linewidth = 1/2)

for i in range(ms):
    if i < 10:
        plt.plot(WLS[i,:, 0], WLS[i, :, 1], 'b', linewidth = 1/2)
        plt.plot(WRS[i,:, 0], WRS[i, :, 1], 'b', linewidth = 1/2)

plt.plot(p[0], p[1], 'k+', markersize = 15)

plt.xlim([-1.5, 1.5])
plt.ylim([-0.5, 0.5])

plt.xlabel('X')
plt.ylabel("Y")


name = "Stable and Unstable Manifold original, for a, b = " + str(a) + " , " + str(b) + ".png"
plt.savefig("Better pictures/Stable and Unstable Manifold/"+name, dpi = 350)
```

References

Alligood, K. T., Sauer, T., & Yorke, J. (1996). *Chaos: An introduction to dynamical systems* (1st ed.). Springer.

Benedicks, M., & Carleson, L. (1991). The dynamics of the Hénon map. *Annals of Mathematics*, *133*, pp. 73–169.

Benedicks, M., & Carleson, L. (1985). On iterations of $1 - ax^2$ on $(-1, 1)$. *Annals of Mathematics*, *122*, pp. 1–25.

Benettin, G., Galgani, L., Giorgilli, A., & Strelcyn, J. M. (1980). Lyapunov characteristic exponents for smooth dynamical systems and for hamiltonian systems; a method for computing all of them. part 1: Theory. *Meccanica*, *15*, pp. 9–20.

Broer, H., & Takens, F. (2009). *Dynamical systems and chaos* (1st ed.). Epsilon Uitgaven.

de Snoo, H., & Winkler, H. (2023). Lecture notes probability and measure. *University of Groningen*.

Devaney, R. L. (2003). *An introduction to chaotic dynamical systems* (2nd ed.). Westview Press.

Devaney, R., & Nitecki, Z. (1979). Shift automorphisms in the Hénon mapping. *Communications in Mathematical Physics*, *67*, pp. 137–146.

Eckmann, J. P., & Ruelle, D. (1985). Ergodic theory of chaos and strange attractors. *Reviews of Modern Physics*, *57*, pp. 617–656.

Filip, S. (2017). Lecture notes on the multiplicative ergodic theorem. *University of Chicago*.

Frederickson, P., Kaplan, J., Yorke, E., & Yorke, J. (1983). The Liapunov dimension of strange attractors. *Journal of differential equations*, *49*, pp. 185–207.

Gallas, J. A. C. (1993). Structure of the Parameter Space of the Hénon Map. *Physical Review Letters*, *70*, pp. 2714–2717.

Garst, S. (2018). *Dynamics amidst folding and twisting in 2-dimensional maps.* (Doctoral dissertation). Rijksuniversiteit Groningen.

Grassberger, P., & Procaccia, I. (1983). Measuring the strangeness of strange attractors. *Physica D: Nonlinear Phenomena*, *9*, pp. 189–208.

Hénon, M. (1976). A two-dimensional mapping with a strange attractor. *Communications in Mathematical Physics*, *50*, pp. 69–77.

Kaplan, J., & Yorke, J. (1979). Chaotic behavior of multidimensional difference equations. *Lecture Notes in Mathematics, Springer Verlag, New York*, *730*, pp. 204–227.

Lorenz, E. (1963). Deterministic nonperiodic flow. *Journal of the Atmospheric Sciences*, *20*, pp. 130–141.

Lyapunov, A. (1892). The general problem of the stability of motion. *Kharkov Mathematical Society*.

Marotto, F. (1979). Chaotic behavior in the Hénon mapping. *Communication in Mathematical Physics*, *68*, pp. 187–194.

Nusse, H., & Yorke, J. A. (1998). *Dynamics: Numerical explorations* (2nd ed.). Springer New York.

Oseledets, V. (1968). A multiplicative ergodic theorem: Lyapunov characteristic numbers for dynamical systems. *Transactions Moscow Mathematical Society*, *19*, pp. 197–231.

Parker, T., & Chua, L. O. (1989). *Practical numerical algorithms for chaotic systems.* Springer-Verlag New York inc.

Peitgen, H.-O., Jürgens, H., & Saupe, D. (2004). *Chaos and fractals: New frontiers of science* (2nd ed.). Springer-Verlag New York.

Pikovsky, A., & Politi, A. (2016). *Lyapunov exponents: A tool to explore complex dynamics* (1st ed.). Cambridge University Press.

Pugh, C. C. (2017). *Real mathematical analysis* (2nd ed.). Springer.

Rössler, O. (1979). An equation for hyperchaos. *Physics Letters A*, *71*, pp. 155–157.

Russel, D., Hanson, J., & Ott, E. (1980). Dimension of strange attractors. *Physical Review Letters*, *45*, 1975–1978.

Simó, C. (1992). On the analytical and numerical continuation of invariant manifolds. In *Modern methods in celestial mechanics* (2nd ed.). Éditions Frontières.

Smale, S. (1967). Differentiable dynamical systems. *Bulletin of the American Mathematical Society*, *73*, pp. 747–817.
Viana, M. (2014). *Lectures on Lyapunov Exponents* (1st ed.). Cambridge University Press.